Palaeogeography, Palaeoclimatology, Palaeoecology 538 (2020) 109408

Contents lists available at ScienceDirect

Palaeogeography, Palaeoclimatology, Palaeoecology

journal homepage: www.elsevier.com/locate/palaeo

Prosopis sp. tree-ring oxygen and carbon isotope record of regional-scale hydroclimate variability during the last 9500 years in the Atacama Desert

E.J. Olson[a,d,*], J.P. Dodd[a], M.A. Rivera[b,c]

[a] Northern Illinois University, Department of Geology and Environmental Geosciences, Dekalb, IL, USA
[b] Universidad de Magallanes, Punta Arenas, Chile
[c] The Field Museum of Natural History, Chicago, IL, USA
[d] Purdue University, Department of Earth, Atmospheric and Planetary Sciences, West Lafayette, IN, USA

ARTICLE INFO

Keywords:
Climate
Holocene
Early agriculture
ENSO
Andes
South America

ABSTRACT

The hyper-arid core of the Atacama Desert is one of the most persistently arid environments in the world, yet there is evidence of significant hydroclimate variability during the Holocene. The timing of regional scale pluvial or humid periods has important implications for understanding the drivers of South American climate variability as well as the development of agriculture by prehistoric cultures. Here we present oxygen ($\delta^{18}O$) and carbon ($\delta^{13}C$) isotope values from ancient *Prosopis* sp. tree-ring cellulose as a record relative humidity (RH) and water availability (via intrinsic water–use efficiency) over century–long intervals throughout the past 9.5 ka in the northern Atacama Desert (19–21°S). These data provide the first high–resolution (ca. annual) evidence for decreasing water availability and increasing climate variability in the Atacama from the early-to late- Holocene. Intrinsic water–use efficiency steadily increases over the Holocene indicating a lowering of the water table and a reduction in the availability of groundwater resources in the region. As water availability decreases, $\delta^{18}O$-based estimates of RH show increased variance beginning ~4.9 ka. This change in RH coincides with the onset of modern day Central Andean atmospheric circulation patterns and previously documented humid periods in the southern Altiplano (22–24°S). Subannual tree-ring isotope analysis of modern and early Holocene (8.3 ka) trees show a similar seasonal cycle in carbon isotope values that correlates with modern annual changes in temperature; however, the early Holocene interseasonal variability is greater than modern seasonality. $\delta^{18}O$ values of the Atacama tree-rings are highly correlated with those of the Sajama ice core from the Bolivian Andes, demonstrating a teleconnection between high-altitude Andean precipitation and water availability in the Atacama Desert. These reconstructions together provide a record of Holocene water availability and ephemeral recharge related to changes in ENSO and South American monsoon.

1. Introduction

In the coastal and low–elevation regions of northern Chile and southern Peru, limited instrumental data and a paucity of high–-resolution paleoclimate proxies have led to contradicting reconstructions of past climatic and hydrologic conditions (e.g. Grosjean et al., 2003). Paleoclimate records from the Atacama have identified periods of extreme variation in water availability throughout the past 10ka. The early Holocene (11.7–8.2 ka) is generally thought to have been wetter than present with increased pluvial periods associated with Central Andean Pluvial Events (CAPE, Quade et al., 2008). CAPE are documented in numerous lake sediment records in the Altiplano (high-altitude Central Andean plateau), and by the presence of lake and wetland deposits are present within the currently dry Atacama Basin (Grosjean, 2001a; Núñez, 2002; Messerli et al., 1993; Wolfe et al., 2001). It is difficult, however, to determine if the these temporally discontinuous proxies (e.g. paleowetlands, rodent middens and paleosols) record regional scale variations in paleoclimate and groundwater levels. For example, additional proxy records suggest that from 9 to 4 ka the Atacama was more arid than today, with an brief humid interval around 6 ka (e.g. Abbott et al., 2003; Baker et al., 2001; Grosjean, 2001b; Thompson et al., 1998). Most proxy records agree that the late Holocene (4.2 ka – present) was persistently arid, and models of atmospheric circulation over the Central Andes indicate that by 3.0 ka the region resembled modern day conditions (Vuille and Keimig, 2004).

The challenge with interpreting regional-scale trends in Holocene climate across the Atacama is that they appear to be punctuated by abrupt pluvial events (e.g. high humidity, increased groundwater

* Corresponding author. Northern Illinois University, Department of Geology and Environmental Geosciences, Dekalb, IL, USA.
E-mail address: ejolson@purdue.edu (E.J. Olson).

https://doi.org/10.1016/j.palaeo.2019.109408
Received 19 July 2018; Received in revised form 10 October 2019; Accepted 12 October 2019
Available online 23 October 2019
0031-0182/

discharge, formation of wetlands, and rodent midden deposits). Paleovegetation and wetland sedimentation records document at least six pluvial periods in the central Atacama (22–24°S) at approximately 9.8 ka, 9.1 ka, 8.4 ka, 5.1–3.2 ka, 2.8–1.2 ka, and 1.0–0 ka (Bentancourt et al., 2000; Latorre et al., 2003; Grosjean et al., 1997; Rech et al., 2002; Sáez et al., 2016; Pfeiffer et al., 2018a,b). While wetland records from the northern Atacama (19.5–21.5°S) Pampa de Tamarugal basin (PdT basin) provide evidence of humid periods at 9.5 ka, 8.8 ka, 8.3 ka, 7.8–7.7 ka, 6.7 ka, 1.1–0.9 ka, 0.86 ka, and 0.78–0.71 ka (Nester et al., 2007; Gayo et al., 2012; Blanco and Tomlinson, 2013; Tomlinson et al., 2015; Pfeiffer et al., 2018a,b). The temporal discordance between the northern and central Atacama records is attributed to differential mixing of moisture sources throughout the Holocene (Pfeffier et al., 2018a,b). Such differences in the dominant moisture source are observed in the modern period with rainfall being sourced from the Amazonian Basin in the north and from the Pacific and SE Atlantic in the central Atacama (Vuille and Keimig, 2004; Houston, 2006; Quade et al., 2008). Whether this modern geographic divide in Atacama precipitation source can be applied to the past cannot be resolved from the currently available proxy records. However, recent spatial analysis of rodent middens from 22 to 24°S by de Porras et al. (2017) suggest that the prevailing moisture source difference between the northern and southern Atacama regions is present as early as the late Pleistocene-Holocene transition.

The hyper–arid Atacama Desert core (18–24 °S) naturally preserves tree trunks without fossilization. Radiocarbon (^{14}C) dates on ancient tree samples of various species recovered from the Atacama Desert are as old as 15 ka (Gayo et al., 2012; Latorre et al., 2013). In the PdT Basin (19–21 °S), *Prosopis tamarugo* are the dominant forest species for which the basin is named; however, a number of other *Prosopis* sp. have also been extensively studied (e.g. Gomes and Bolzon de Muniz, 1988; Flinn et al., 1994; Lopez et al., 2005). The presence of both living and ancient *Prosopis* sp. in this region allows for proxy calibration. Additionally, *Prosopis* sp. trees produce annual rings, and provide the opportunity to study the Holocene Atacama Desert climate system over discontinuous intervals at a higher resolution than ever before. Here we provide evidence that *Prosopis* sp. provide a reliable climate proxy for the Atacama Desert and argue that additional development of similar arid tree–ring proxies can greatly enhance understanding of climatic changes in proxy poor arid regions globally. Additionally, the high-resolution tree-ring record presented here spans multiple millennia and provides the opportunity to investigate the timing of hydroclimate variability throughout the Holocene.

1.1. Site description

The Pampa del Tamarugal (PdT) is a semi-enclosed basin in the central valley of the Atacama Desert (19° 17′–21° 50′S, 950–1200 m a.s.l.). This hyper-arid region receives less than 1 mm of rainfall annually (Houston, 2006) and sedimentological deposits suggest it has been arid since the Miocene (Hartley, 2003; Rech et al., 2003; Ewing et al., 2006; Jordan et al., 2014; Pfeiffer et al., 2019). The aridity of the Atacama is controlled by the Hadley-circulation-driven high-pressure belt of dry sub-tropical air descending between 15° and 30° S, and the upwelling of the cold polar waters via the Peruvian Current along the west coast. Together, these factors create an inversion layer (warm air overlaying cold air) preventing moisture advection to the region. Endemic *Prosopis* sp. trees grow in isolated stands dispersed across this otherwise barren landscape with only a few succulent and shrub-level species. *Prosopis* sp. trees can grow up of 25 m in height and rely on shallow groundwater < 20 m below the surface to survive, and < 5 m for juvenile growth (Mooney et al., 1980; Trobok, 1984; Chávez et al., 2013, 2016; Calderon et al., 2015).

Annual rainfall averages 60–200 mm per year in the Andean Altiplano (elevations above 2300 m a.s.l.) (Aceituno, 1988; Houston and Hartley, 2003). These rains in the Andes to the east of the PdT recharge groundwater in the basin via stream and shallow groundwater flow during heavy rainfall events and through deep-seated fractures along longer flow paths (Margaritz et al., 1990; Aravena, 1995; Jayne et al., 2016; Scheihing et al., 2018). Rainfall in the western Andean Altiplano occurs seasonally during austral summer (DJF) when strong upper level easterly winds transport moisture from the Amazon basin via deep convective cells (Garreaud et al., 2003). These rainfall events represent the southernmost extent of the South American Summer Monsoon (SASM) (Zhou and Lau, 1998). Modern–day hydroclimate in the northern Atacama (above 23ºS) is strongly linked to El Niño – Southern Oscillation (ENSO) variability (Vuille and Keimig, 2004). Strengthening (weakening) of the westerly winds during the El Niño (La Niña) ENSO phase blocks (enhances) easterly moisture (i.e. SASM rainfall), and results in dry (wet) conditions in the Altiplano (Vuille, 1999; Garreaud, 2000; Vuille et al., 2003a,b).

Source water for the phreatophyte *Prosopis* sp. in our study region are limited to groundwater and fluvial runoff sourced from the higher elevation regions in the Andean foothills to the east. Groundwater recharge events over the modern observational period are infrequent with decadal to centennial recurrence (Houston, 2006). Groundwater $\delta^{18}O$ values range between −14 and −6‰ (VSMOW) within the PdT basin (Fritz et al., 1981; Margaritz et al., 1989; Alpers and Whittemore, 1990; Aravena and Suzuki, 1990) and have not changed significantly over the period of modern observation (e.g. 1970s to present; Jayne et al., 2016). Less common pluvial events are thought to have recharged the PdT aquifer with millennial frequency (Gayo et al., 2012). Indeed, ^{14}C dating of groundwaters in the basin below 1400 m a.s.l. show residence times ~1284 years BP (Scheihing et al., 2017).

1.2. Dual isotope δ18O and δ13C approach

Stable isotope dendroclimatology requires fewer trees to obtain a strong common climate signal than ring-width measurements (Robertson et al., 1997a,b; McCarroll and Pawellek, 1998). Due to the lower sample numbers required, tree-ring isotopic data have extended the utility of tree–ring records where few individual trees are available, and extended the temporal reach of such records to geologic periods as ancient as 45 million years ago (e.g. Jahren and Sternberg, 2003; Jahren and Sternberg, 2008). Additionally, the ability to subsample rings facilitates the quantitative assessment of changes in environmental factors such as temperature and relative humidity (RH) at higher temporal resolution (e.g. Dodd et al., 2008; Schubert et al., 2012). Such paleoclimate records are typically from polar regions where persistently cold dry conditions have mummified wood remains without fossilization (eg. Ballantyne et al., 2006; Hook et al., 2013; Hook et al., 2014). In rare cases, the preservation of entire swaths of forests has even facilitated the cross–dating of trees and the development of statistically robust annually–resolved records of temperature (e.g. Csank et al., 2013). Other exceptions are late Pleistocene records from temperate regions such as southern France (Pauly et al., 2018), the Great Lakes region (Leavitt, 2012), and midcontinental North America (Voelker et al., 2015). Arid regions similarly have high preservation potential; however, unlike polar regions these climates lack traditional forest biomes and as a result lack the sample quantity for traditional dendrochronological ring-width studies. Previous research on stable isotope variability in arid *Tamarix jordanis* trees from Israel (Yakir et al., 1994; Lipp et al., 1996; Frumkin, 2009) has demonstrated the utility of arid tree species in paleoclimate reconstructions despite low sample availability (using as few as one tree per study site). In arid environments, the low number of samples necessary to obtain a strong climatic signal, as compared to temperate or tropical climates, is due to the absence of forest canopy dynamics and limited water sources.

The $\delta^{18}O$ value of cellulose is largely controlled by the isotopic composition of the water utilized in cellulose synthesis (Barbour, 2007). In the absence of precipitation, the PdT, *Prosopis* sp. trees today grow solely on groundwater. Given the stable aridity of the Atacama over the

Holocene, we can assume that groundwater was the dominate tree-water source in the past. Therefore, the $\delta^{18}O$ tree-ring record presented here provides a history of the groundwater $\delta^{18}O$ during tree growth. Temporal changes in the groundwater $\delta^{18}O$ values are ultimately the product of atmospheric processes (e.g. Rayleigh distillation and temperature driven fractionation) and precipitation source (e.g. Dansgaard, 1964). Groundwater recharge in arid regions, however, is not instantaneous, and observed changes in groundwater $\delta^{18}O$ values may lag behind atmospheric conditions. Previous research in the PdT observed that recharge events in the highlands take an average of 20–24 months to reach the eastern edge of the basin (Scheihing et al., 2017), and would take an average of ~3 years to reach our study areas assuming constant flow rate. Analysis of central Andean precipitation and ice core data by Vuille and Werner (2005) demonstrate that while moisture is sourced from the tropical Atlantic via the SASM, the $\delta^{18}O$ value of precipitation in the central Andes interannually is related to the dampening of SASM strength by ENSO. The combined imprint of SASM and ENSO strength on central Andean precipitation isotope values provides a means by which paleo-precipitation in the Atacama can be investigated. Tree–ring isotope records from this region provide an opportunity to understand the frequency and intensity of these previously identified pluvial/humid periods at higher-resolution and comparison with equally detailed isotope records from other regions of South America. Additionally, the sub-annual sampling of *Prosopis* sp. tree rings allows for reconstruction of variability at a scale that can resolve processes such as the SASM and ENSO.

Carbon isotope ($\delta^{13}C$) values of cellulose can bolster the identification of pluvial events and humid episodes since both isotope systems respond to changes in vapor pressure deficit. Molecular CO_2 is larger than H_2O, and in order for plants to take up carbon they must lose water via transpiration. Leaf stomata conductance links both isotope systems, though the relationship between the two values is not straightforward since alterations in RH can be masked by changes in temperature, sun light, nitrogen and water availability (Roden and Farquhar, 2012).

In the arid Atacama Desert we can make several assumptions regarding these variables in the case of *Prosopis* sp. First, sun light is not a limiting factor to tree growth since there is no forest canopy to overcome and cloud cover is limited. Secondly, nitrogen availability remains relatively consistent, and nutrient derived fractionation of $\delta^{13}C$ values is negligible. In part, this is because *Prosopis* species fix nitrogen from the atmosphere, and the Atacama is covered in nitrate salt deposits. Lastly, in this harsh desert climate these phreatophytes cannot live without groundwater, thus changes in water availability in the tree-ring isotope timeseries never record the complete absence of groundwater. These unique conditions provide a simplified scenario in which the dual–isotope approach can be applied in order to identify the intensity and frequency of humid events and shifts in Atacama hydroclimate during the Holocene.

Annually and subanually resolved tree–ring $\delta^{18}O$ and $\delta^{13}C$ values from *Prosopis* sp. trees reported here were collected from surface deposits and archaeological sites in the Pampa del Tamarugal (PdT) Basin of northern Chile (Fig. 1). This record of ancient trees is compared to a modern record of *Prosopis* sp. trees from the Salar de Llamara. Samples dating between 9.8 and 7.7 ka also come from the Salar de Llamara, while those dating from 4.9 to 1.8 ka were recovered from the archaeological sites of Guatacondo, Ramaditas and Casarones. Comparison of the ancient tree-ring isotope records to other regional precipitation proxies demonstrates significant changes in atmospheric moisture throughout the Holocene in the northern Atacama.

2. Methods

The hardness and density of *Prosopis* sp. makes sampling these trees difficult. In order to collect samples, disks of wood were cut using a chainsaw. In cases where the chainsaw method was not feasible, a custom–made, dendrochronological borer (Pressler© GmbH), fitted to a battery- or gas-powered drill was deployed (Krottenthaler et al., 2015). Both modern and ancient samples were collected in field between 2012 and 2017 (Fig. 2). Samples from the archaeological sites of Ramaditas, Caserones, and Guatacondo were collected by Mario Rivera during archaeological excavations. Ancient tree samples may have been moved by humans in the past, for this reason the records are treated as representative of the PdT basin over the Holocene and smaller scale dynamics (eg. proximity to quebrada, lake, hill slope, etc.) are not discussed.

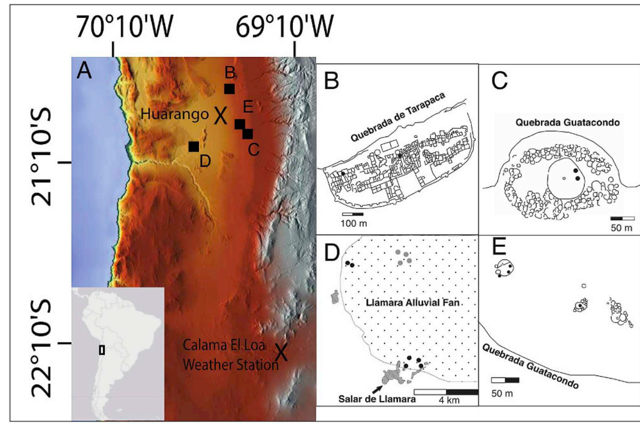

Fig. 1. Study area map with sampling site locations (A). Archaeological sites with tree sample locations marked by black squares for Caserones (B), Guatacondo (C), and Ramaditas (E). The ancient trees sampled at Salar de Llamara marked by black circles and the modern samples by gray circles (D).

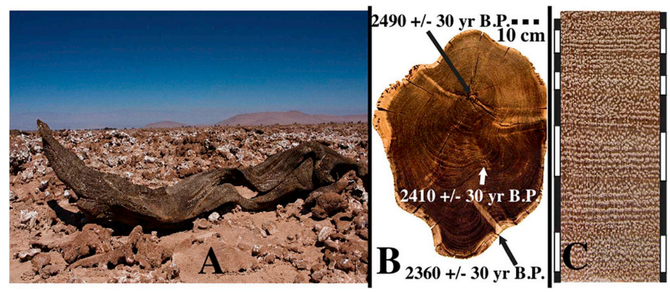

Fig. 2. A) Llamara sample site with ancient tree IGSN: IE18O000F on surface and living trees in background. B) Cut disk of sample IGSN: IE18O000A ancient tree from Ramaditas site with ^{14}C dates. C) Close up of rings from sample in B showing that along transects rings are parallel.

Ancient trees were ^{14}C dated following cellulose extraction and secondary solvent rinses using accelerator mass spectrometry (AMS) at Beta Analytic and the Keck Carbon Cycle AMS Facility, Earth System Science Dept, UC Irvine. All ^{14}C dates were corrected using the OxCal4.2 program (https://c14.arch.ox.ac.uk/embed.php?File=oxcal.html) and the Southern Hemisphere calibration curve (SHcal13) by Hogg et al. (2013). For trees with multiple ^{14}C dates, the tree–ring sequence model with ring counts was used to assign each date to the corresponding ring with better accuracy (Ramsey et al., 2001). For ancient specimens, the ^{14}C date for each individual ring is an estimate based on the mid–point of the date two–sigma range. For trees with multiple dates the midpoint of the two–sigma range for each date was assigned to the corresponding ring. A high–resolution photograph of a tree disk with multiple dates is shown in Fig. 2.

A total of 1747 annual and 106 subannual ring samples from 24 individual trees were analyzed for carbon and oxygen isotope values. Ring identification and annual sampling was conducted on sanded disks/cores using a binocular microscope (7–45× magnification) using a Foredom TX-series flexible shaft rotary power tool with variable speed control. Subannual samples were obtained using a microtome to section individual rings at sub-millimeter scale. Extraction of α–cellulose from individual tree-ring samples was conducted using the Brendel et al. (2000) method modified for small samples (Anchukaitis et al., 2008; Evans and Schrag, 2004). Carbon and oxygen isotope values were measured via continuous flow isotope ratio mass spectrometry (IRMS) on a Thermo MAT253 coupled with a TC/EA in the Stable Isotope Laboratory at Northern Illinois University (SIL-NIU). Carbon isotope values were corrected for the difference in values between combustion and pyrolysis by reanalyzing a subset ($n = 297$) of samples via on–line combustion on a Costech EA system coupled to a Thermo DeltaXL IRMS and applying a linear correction (Woodley et al., 2011). The α–cellulose samples and standards were homogenized, and vacuum dried overnight prior to analysis. The reported oxygen and carbon values are in per mil (‰) relative to VSMOW and VPDB (respectively) based on corrections to international standards of α–cellulose IAEA–CH3 ($\delta^{18}O = 32.2 \pm 0.2$‰; $\delta^{13}C = -24.7 \pm 0.2$‰; $n = 119$) and benzoic acid IAEA–601 ($\delta^{18}O = 23.3 \pm 0.29$‰; $\delta^{13}C = -28.81 \pm 0.26$‰; $n = 119$) for pyrolysis and IAEA–CH3 ($\delta^{13}C = -24.7 \pm 0.1$‰; $n = 30$) and benzoic acid IAEA–601 ($\delta^{13}C = -28.81 \pm 0.06$‰; $n = 30$) for combustion analyzed every ten samples to monitor intra–run variability. Analytical precision was determined by an internal laboratory standard of Sigma–Aldrich α–cellulose ($\delta^{18}O = 31.9 \pm 0.3$‰; $\delta^{13}C = -25.2 \pm 0.3$‰; $n = 155$).

Leaves were collected from ~1.5 m above surface from healthy tree limbs. Leaves were analyzed for $\delta^{13}C$ via combustion on a Costech EA and Thermo IRMS at the University of Cincinnati. Values were normalized to the VDPB scale, using in-house standards and precision was 0.3‰ (1σ, $n = 10$).

Ancient carbon isotope values were corrected using $\delta^{13}C$ and CO_2 concentration values for atmospheric air throughout the Holocene measured in Antarctic ice cores (Elsig et al., 2009). Modern $\delta^{13}C$ values were correcting using CO_2 concentration data from the Moana Loa observation station and $\delta^{13}C_{air}$ data from McCarroll and Loader (2004) interpolation of measured values in Francey et al. (1999). There has been discussion in the literature on how to correct for changes in the CO_2 concentration of the atmosphere (Treydte et al., 2016; McCarroll et al., 2009). Here we applied a linear correction as recommended by Schubert and Jahren. (2011).

Intrinsic water–use efficiency (iWUE) was calculated using the formula:

$$iWUE = c_a\left[1 - \left({c_i}/{c_a}\right)\right](0.625) \tag{1}$$

Where c_a and c_i are the atmospheric and internal leaf concentration of CO_2 respectively and the ratio between them is determined by the equation below:

$${c_i}/{c_a} = (\delta^{13}C_{plant} - \delta^{13}C_{air} + a)/(b - a) \tag{2}$$

In equation (2), fractionation factors, a (– 4.4‰) is discrimination against $^{13}CO_2$ diffusion of CO_2 through the leaf stomata and b (–28.3‰) is due to preferential use of ^{12}C during carboxylation (Farquhar and Richards, 1984; Schubert and Jahren, 2013). $\delta^{13}C_{plant}$ is the value of bulk leaf carbon which for *Prosopis* sp. is -25.91‰ $\pm$ 0.91 ($n = 22$) and differs on average from wood cellulose (-24.31‰ $\pm$ 0.65) by 1.69‰ this correction factor is added to compensate for the difference (McCarroll and Loader, 2004).

Average basin RH is estimated for each period using the equation from Anderson et al. (2002):

$$\delta^{18}O_{sw} \approx \delta^{18}O_{cell} - (1 - f) \times (1 - h) \times (\varepsilon_e + \varepsilon_k) - \varepsilon_{biochem} \tag{3}$$

Solving this equation for h [fx], RH, and assuming the dampening factor due to exchange of cellulose with source water ($f = 0.42$, Roden et al., 1999), the liquid–vapor equilibrium fractionation for water at average photosynthetic temperature 21.4 °C ($\varepsilon_e = 9.44$ Majoube, 1971; Helliker and Richter, 2008), leaf boundary fractionation ($\varepsilon_k = 21$‰, Cernusak et al., 2003) and biosynthetic ($\varepsilon_{biochem} = 27$‰, Sternberg and Deniro. (1983) fractionation are constant. We derive the following equation:

$$h \approx 1 + \frac{Avg.\ \delta^{18}O_{sw} - \delta^{18}O_{cell} + \varepsilon_{biochem}}{(1 - f)(\varepsilon_e + \varepsilon_k)} \tag{4}$$

Modern comparative datasets come from the closest weather station on the plateau in the city of Calama 200 km south of our study region (Direccion de Meteorlogia de Chile). A short–term dataset spanning 2015–2016 comes from a weather station we installed within the basin at the El Huarango field site. Weather station data at the two sites is compared and differences between them are taken into account.

3. Results

3.1. Modern tree series

Analyses of $\delta^{18}O$ α-cellulose indicate that *Prosopis* sp. ring and subring series record changes in climatic conditions over the modern study period (1954–2016). Oxygen isotope ($\delta^{18}O$) values for the modern series average 32.2 $\pm$ 1‰ (VSMOW). The inter–series oxygen correlation coefficient is 0.77 and the series has a negative trend of 2‰ over the modern period (Fig. 3A). Since the ancient data do not have overlapping trees with which to build a mean chronology, correlations between observed climate data over the modern period were done using each individual tree series. Individual ring $\delta^{18}O$ correlates positively with relative humidity and precipitation, and negatively with temperature from the Calama weather station. Stronger correlations between these climate variables and the ten–year averages of $\delta^{18}O$ ring-cellulose values from individual trees produced useful results for paleoclimate proxy application (Table 1). The ten–year averages of PdT RH estimates and observed Calama RH is highly correlated ($r = 0.78$, $p < 0.0001$, $n = 21$, Fig. 4). The standard error, between observed and tree-ring estimated relative humidity, h, is 4.5%. The Calama and PdT weather station temperature also correlated over the period of overlap between datasets 2014–2016 ($r = 0.90$, $p < 0.0001$, $n = 26$).

Modern *Prosopis* sp. series carbon isotope ($\delta^{13}C$) α-cellulose values are sensitive to changes in climatic conditions over the modern study period. $\delta^{13}C$ values for the modern series average -24.3 ± 0.6‰ VPDB (Fig. 3B). The inter-series $\delta^{13}C$ correlation coefficient is 0.16, and no juvenile or long–term trend is observed in the data series. Individual $\delta^{13}C$ values did not correlate with any annual climate variables. The ten–year average of individual tree $\delta^{13}C$ values and observed climate variables produced no significant correlations. However, intrinsic water–use efficiency (iWUE) averaged over decades derived from individual tree $\delta^{13}C$ series correlates with temperature and RH. Over the modern 57-year proxy calibration period (1960–2017) iWUE derived from the mean $\delta^{13}C$ series increases by 40%. The increase in iWUE did not correspond to an increase in tree growth (Fig. S2). This trend in annual iWUE over the modern period correlates with an overall decrease in relative humidity ($r = -0.36$, $p < 0.0001$, $n = 24$) and increasing PdT basin water table depths ($r = 0.85$, $p < 0.0001$, $n = 24$).

Subannual sampling of modern tree rings show no cyclical seasonal trend in $\delta^{18}O$ values. Inter-ring $\delta^{18}O$ values correlate with changes in soil moisture ($r = -0.81$, $p = 0.03$, $n = 6$) from the basin weather station (Fig. 4). The average intra-ring difference for oxygen is 0.2‰ and range from 0.1 to 1.3‰. Subannual $\delta^{13}C$ values exhibit a cyclical pattern annually with a distinctive midseason peak (Fig. 5). Subannual (intra-ring) $\delta^{13}C$ values correlate with changes in temperature ($r = -0.74$, $p = 0.05$, $n = 6$) from the basin weather station. The maximum intra-ring difference in $\delta^{13}C$ values ranges from 0.3 to 1.1‰ for the five

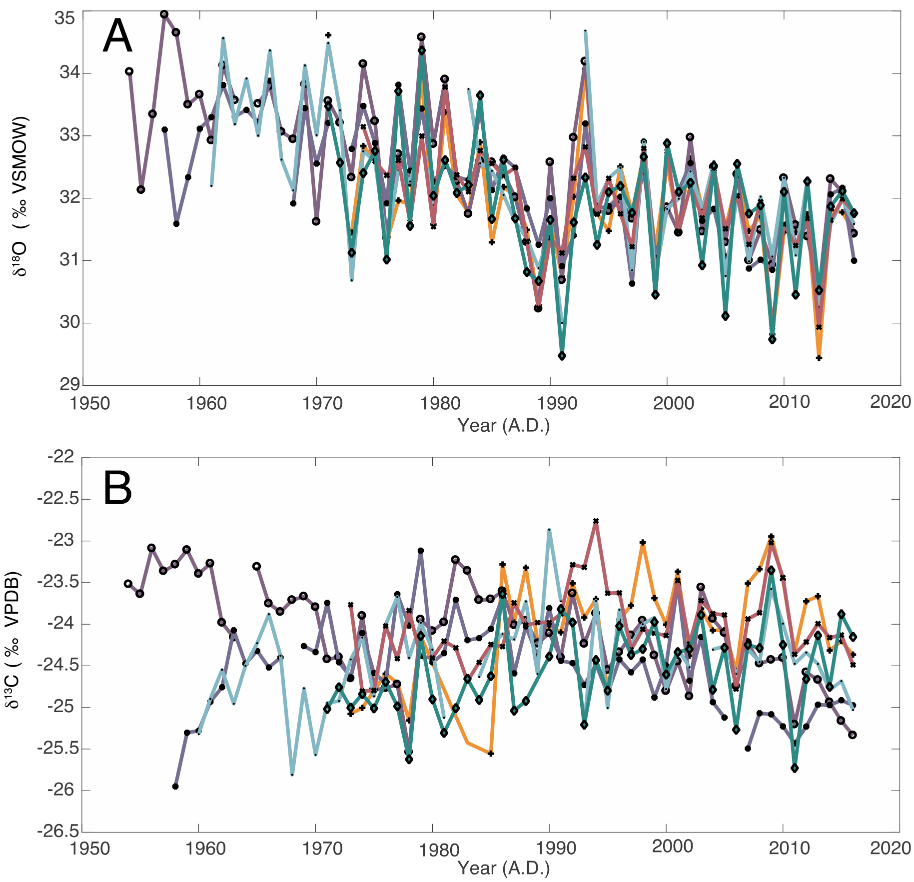

Fig. 3. Modern annual $\delta^{18}O$ (A) and $\delta^{13}C$ (B) series plots.

trees sampled and averages 0.6‰. *Prosopis* sp. sampled in this study record a subannual increase in $\delta^{13}C$ values rhar occurs mid-ring as previously observed in evergreen (Schubert and Jahren, 2011) and tropical tree species (Poussart et al., 2004; Fichtler et al., 2010).

3.2. Ancient tree series

Oxygen and carbon annual isotope data of ancient tree samples are summarized in Table 2. The $\delta^{18}O$ values increase steadily in the early Holocene period from 9.7 to 8.3 ka (Fig. 6). Inter-ring $\delta^{18}O$ variability is lowest at 7.7 ka and highest at 1.9 ka (Fig. 6). Intra-ring $\delta^{18}O$ values for sample IGSN: IE18O000E range from 0.9 to 2.2‰ and average 1.36‰ (Fig. 7). RH estimates based on $\delta^{18}O$ values remain near the modern average with changes in variance throughout the Holocene (Fig. 8A). The largest range in RH estimates from annual ring data are observed between 4.9 and 1.9 ka from archaeological tree samples and the smallest range occurs at 7.7 ka at the Salar de Llamara site.

Average $\delta^{13}C$ values are variable throughout the Holocene with notable increases in isotope values at 8.3 ka and 2.0 ka. $\delta^{13}C$ values trend toward higher values in the younger samples, although inter–-annual variability peaks at 8.3, 4.9, and 1.9 ka. Subring $\delta^{13}C$ values for sample IGSN: IE18O000E range from 1.2 to 1.9‰ and average 1.7‰.

Intrinsic water–use efficiency (iWUE), is the ratio of plant water-used to water-lost during carbon-fixation (Farquhar and Richards, 1984; Ehleringer, 1993). iWUE is derived from $\delta^{13}C$ values ranges between 40 and 50 from 9.6 to 8.6 ka and increases (~55–60) at intervals between 8.5 and 8.3, 2.5–2.4, and 1.9–1.8 ka. The ancient iWUE values are generally lower than those of the modern trees for which iWUE values range from 50 to 95. The lowest value for iWUE is from the sample dating to 7.7 ka with an average of 47 (Fig. 8B). Ring-width measurements from the modern and ancient trees show no linear trend with age or isotope values (Fig. S1).

4. Discussion

4.1. Modern Prosopis sp. RH estimates and iWUE

Decadal averages of tree-ring-isotope based calculations of RH and iWUE provide a strong analogue that facilitates the interpretation of the ancient *Prosopis* sp. isotope data. The decadal averaging of individually run series provides a direct comparison to the available data from ancient *Prosopis. sp* trees; however, this approach severely decreases the sample size and the validation of relationships via an independent dataset is not possible. To address this issue, we critically evaluate these

Table 1
Modern series correlation coefficient (*r*) for decadal 10-year annual data averages and individual ring values of all modern tree samples. Temperature, relative humidity and precipitation data are from the Calama weather station. All bold values are statistically significant $p < 0.05$.

	10-yr Avg. $\delta^{18}O_{ac}$	Individual rings $\delta^{18}O_{ac}$	10-yr Avg. $\delta^{13}C_{ac}$	Individual rings $\delta^{13}C_{ac}$	iWUE	10-yr Est. RH (*h*)
Temperature	**−0.95**	**−0.46**	0.11	0.00	**0.60**	**−0.95**
Relative Humidity	**0.78**	**0.24**	0.04	0.05	**−0.37**	**0.78**
Precipitation	**0.55**	**0.15**	0.02	0.03	0.10	**0.55**

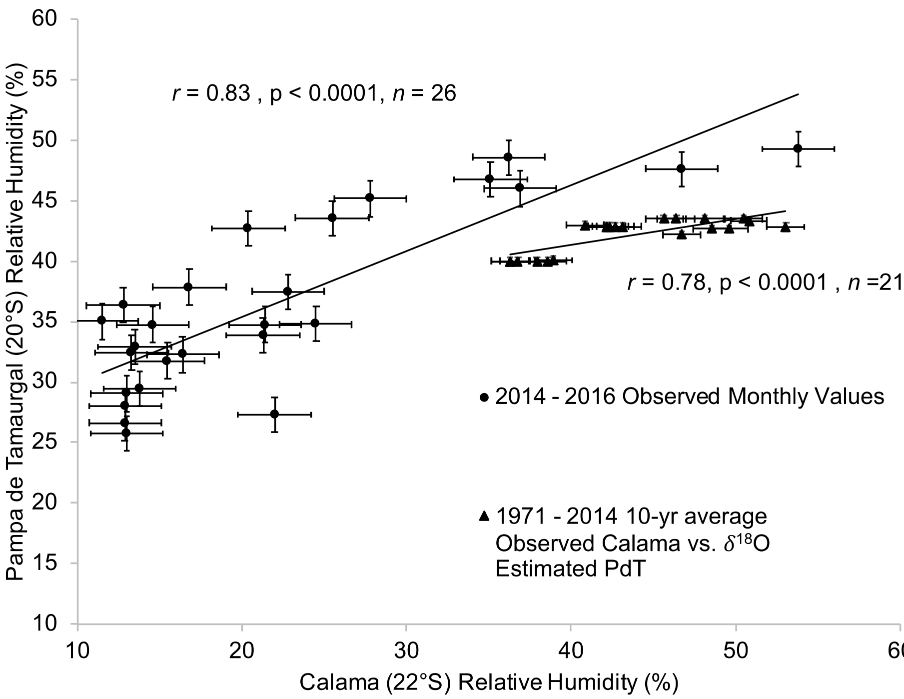

Fig. 4. Modern correlation between observed Pampa de Tamarugal (20°S) and Calama (22°S) relative humidity from weather stations (circles) representing monthly average of instrumental dataset at each site from November 2014–December 2016. Error bars represent reported instrument accuracy. PdT relative humidity estimated from $\delta^{18}O$ α-cellulose values and observed weather station relative humidity from Calama, Chile (triangles). Triangles represent ten-year average of weather station data and individual tree series $\delta^{18}O$ ten-year relative humidity estimates. Error bars represent the standard deviation of both variables over the interval.

relationships with respect to current understanding of tree-ring isotopic fractionation and the standard error is provided for iWUE and RH data.

The modern data show that both $\delta^{18}O$ and $\delta^{13}C$ values provide a strong analogue for the ancient *Prosopis* sp. interpretations. Specifically, the relationship between the Calama weather station data and conditions on the PdT plateau tree-ring relative humidity series show that there is a correlation between basin RH and $\delta^{18}O$ relative humidity estimates (h). The cold Peruvian Current off the coast of Iquique creates a thermal inversion layer where atmospheric temperatures are colder at sea level and warmer at elevation on the PdT. This thermal inversion layer prevents mixing between the two regions. Modern day cloud cover in the basin peaks is relatively low overall with annual maximum coverage around ~15% (Cereceda et al., 2008). Short–term observations of fog occurrence in the PdT indicate that inland fog occurrences may be induced by solar radiation wherein evaporation of PdT surface waters (i.e. saline lakes, spring oases, etc.) increases in response to radiative heat flux with little or no inundation of coastal fog (Cereceda et al., 2002). For this reason, the fluctuations in relative humidity

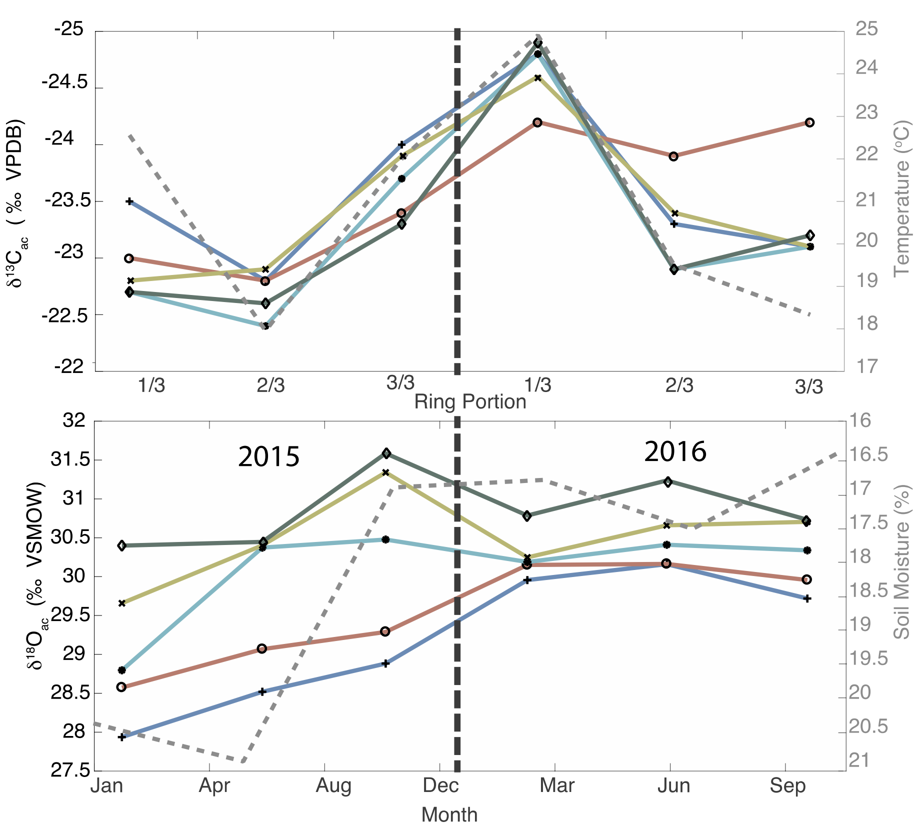

Fig. 5. Modern subannual $\delta^{13}C$ (top) and $\delta^{18}O$ (bottom) values for five individual trees (colored lines) with correlating climatic variables (gray dotted lines). The boundary between years is marked by the vertical line in each plot. Climate data and tree samples are from the El Huarango sampling site. The months on the x-axis are approximate assuming ring growth begins in austral summer during the high-altitude rainy season, as has been observed in other west coast South American *Prosopis* sp. (López et al., 2005). Carbon values are highest in the center of each ring while oxygen shows no apparent annual cycle.

Table 2
Ancient tree series ^{14}C dates and summary isotope data.

Sample IGSN	Measured Age (yr BP)	Ring Dated	Location	2σ SHCal(cal yr BP)	$\delta^{18}O_{ac}$ avg$_{(‰)}$	$\delta^{18}O_{ac}$stdev	$\delta^{13}C_{ac}$avg (‰)	$\delta^{13}C_{ac}$stdev	Number of Rings
IE18O0005[a]	1940 ± 30	Outer	Ramaditas	1918–1745	38.1	1.7	−22.5	0.9	68
IE18O0007	2050 ± 30	Outer	Caserones	2015–1895	32.6	1.2	−22.8	0.4	81
IE18O0006	2090 ± 30	Outer	Guatacondo	2090–1930	36.1	1.2	−21.3	0.5	32
IE18O0008[a]	2100 ± 30	Outer	Caserones	2095–1930	32.5	1.1	−22.8	0.3	44
IE18O000A	2360 ± 30	Outer	Ramaditas	2437–2302	38.1	1.3	−22.8	0.2	84
IE18O0001	2360 ± 30	Outer	Ramaditas	2437–2302	34.6	1.4	−23.2	0.1	17
IE18O000A	2410 ± 30	Middle	Ramaditas	2492–2330	–	–	–	–	–
IE18O000A	2490 ± 30	Center	Ramaditas	2548–2358	–	–	–	–	–
IE18O0009[a]	2510 ± 30	Outer	Ramaditas	2715–2379	35.5	1.2	−22.9	0.2	77
IE18O0009[a]	2510 ± 30	Middle	Ramaditas	2715–2379	–	–	–	–	–
IE18O000B	4390 ± 30	Outer	Guatacondo	5025–4850	36.8	1.6	−23.2	0.6	53
IE18O000C	7040 ± 40	Outer	Llamara	7936–7719	32.4	0.5	−23.6	0.3	92
IE18O000D	7495 ± 25	Outer	Llamara	8351–8189	32.4	0.9	−23.8	0.3	77
IE18O000E	7480 ± 40	Outer	Llamara	8359–8179	32.8	0.6	−21.7	0.6	195
IE18O000F	7640 ± 40	Outer	Llamara	8479–8336	31.3	0.7	−23.5	0.3	145
IE18O000F	7980 ± 25	Center	Llamara	8727–8548	–	–	–	–	–
IE18O000G	8205 ± 25	Outer	Llamara	9145–9012	31.2	0.6	−24.6	0.4	234
IE18O000G	8450 ± 30	Center	Llamara	9313–9358	–	–	–	–	–
IE18O000H	8415 ± 25	Outer	Llamara	9475–9302	31.3	0.9	−23.6	0.6	256

[a] Outliers excluded from climate analysis Note: Center is oldest ring, middle is intermediate in age, and outer is the youngest ring.

recorded over the Holocene does not reflect changes in coastal RH but basin RH as it relates to water availability and to changes in solar radiation. While, the occurrence of fog is not well understood in the PdT future studies of water vapor isotope measurements and longer temporal observational periods if RH variability could provide more data with regards to the atmospheric water vapor source in the PdT and primary drivers. Regardless of the cause for modern RH fluctuations in the PdT regions, these data are consistent between both observational data and the *Prosopis* sp. δ^{18}O-based estimates for RH. The modern δ^{18}O decreases over the study period, this trend is likely in part due to changes in groundwater and rooting depth. However, Pfieffer et al. (2018b) suggest that at depths where groundwater is deeper than 5 m below the surface tamarugo trees cannot survive thus; modern water level lowering due to large scale groundwater extraction would rapidly cause tree die off and is not a major influence on the modern δ^{18}O trends.

Intrinsic water–use efficiency (iWUE) derived from δ^{13}C values is a measure of the ratio of carbon fixed to water lost by the plant (Farquhar and Richards, 1984; Ehleringer, 1993). Since plants must lose water to transpiration in order to gain carbon for photosynthesis, the rate of photosynthesis versus stomatal conductance controls water balance in plants (e.g. Leavitt et al., 2003). The modern *Prosopis* sp. iWUE correlates to increasing CO_2, decreasing coastal relative humidity and lowering of basin groundwater depths. Other modern studies have similarly attributed increases in iWUE to increasing CO_2 at dry sites (Bert et al., 1997; Duquesnay et al., 1998; Feng, 1999; Linares et al., 2009; Saurer et al., 2004; Maseyk et al., 2011). Considering the correlation between decadal averages of iWUE and coastal weather station data (Table 1) we observe that, as conditions become more humid/wet iWUE increases. However, since coastal and PdT RH are inversely related this

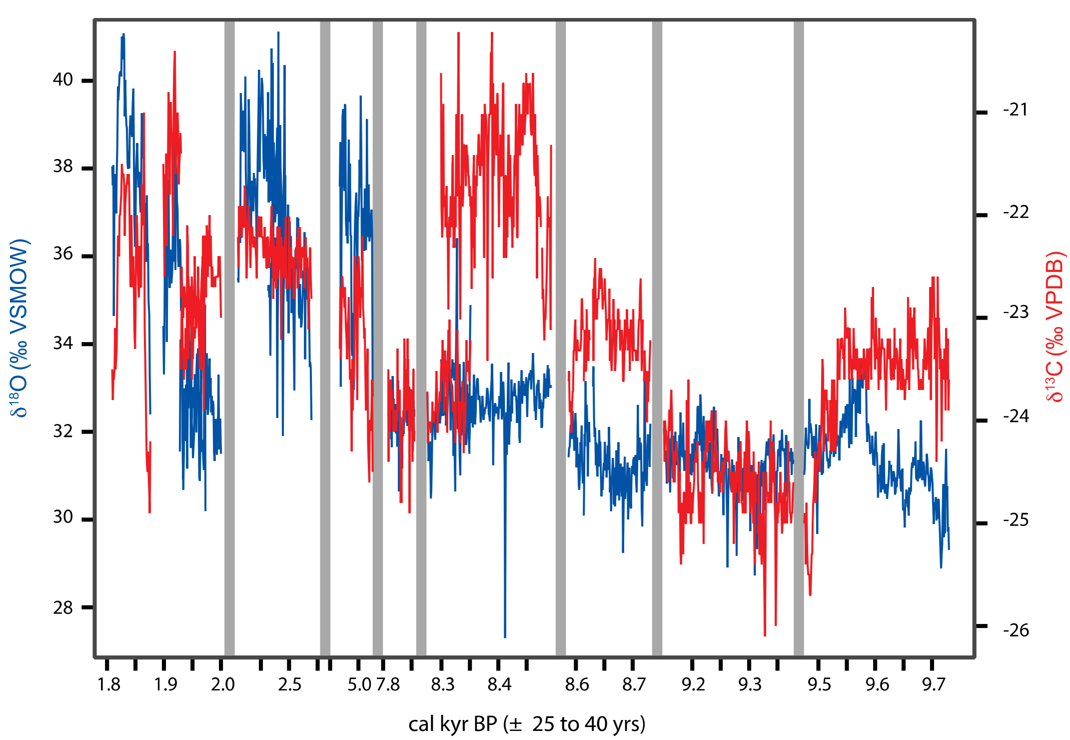

Fig. 6. Early Holocene δ^{18}O (blue) and δ^{13}C (red) *Prosopis* sp. series.

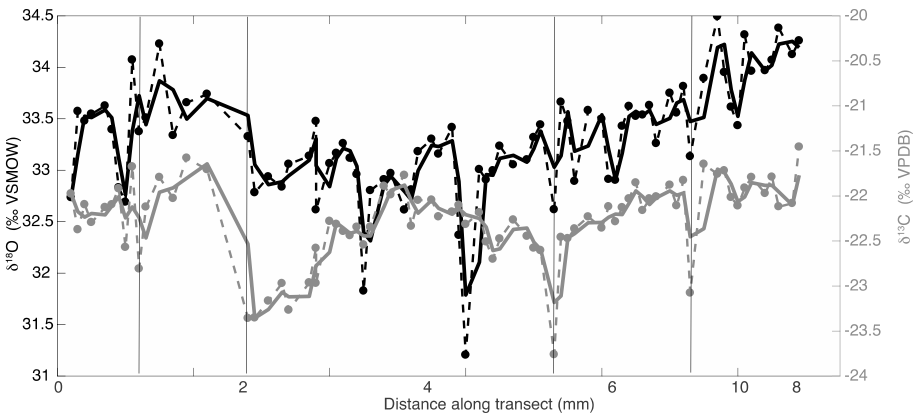

Fig. 7. Ancient subannual $\delta^{18}O$ (black) and $\delta^{13}C$ (gray) values interpolations between measurements are dotted lines and two-point moving averages are solid lines. Vertical lines denote the ring boundary for sample IGSN: IE18O000E dating to 8.2 ka. Carbon values are highest in the center of each ring while oxygen shows no apparent annual cycle.

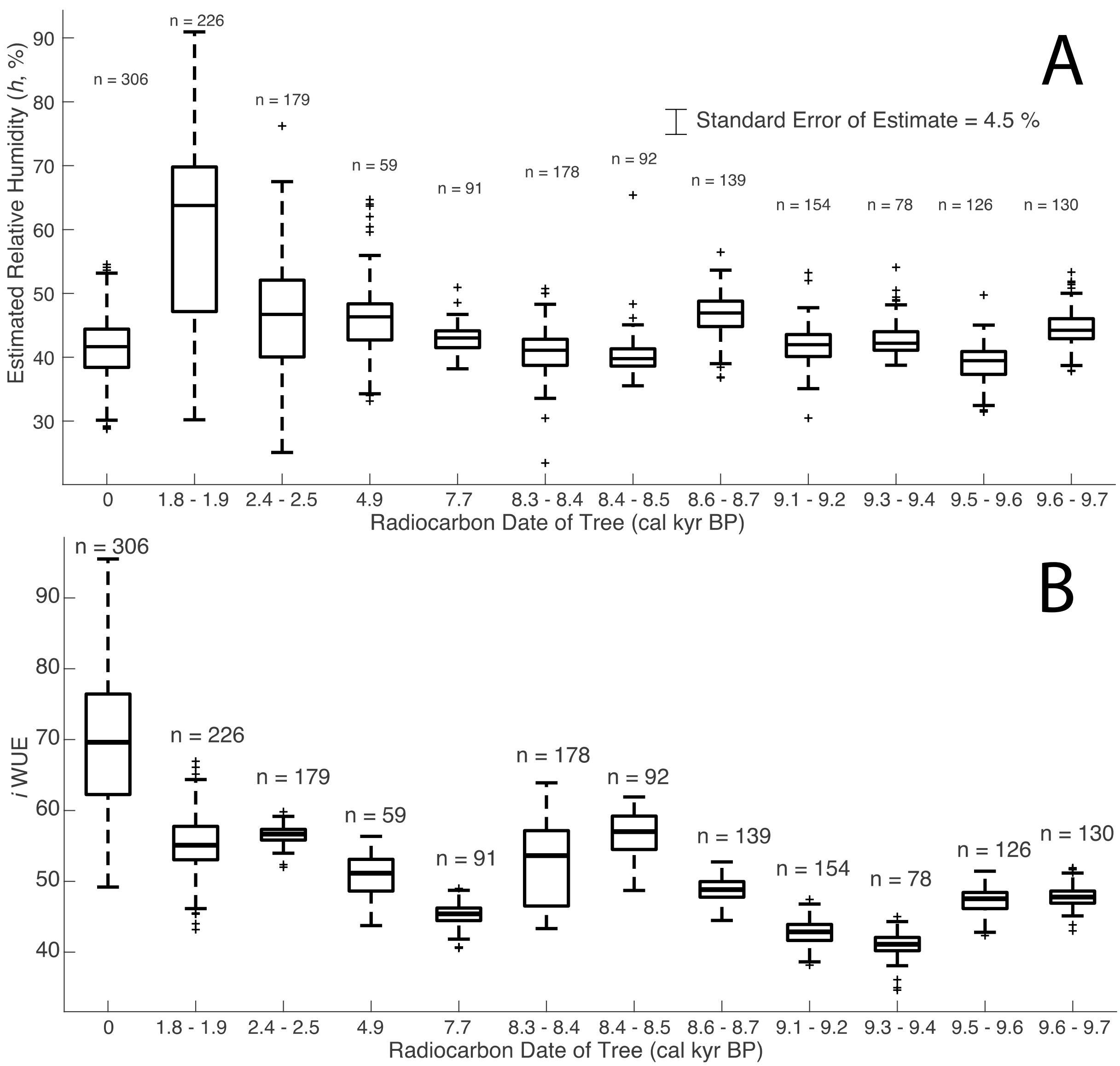

Fig. 8. A) Estimated relative humidity for the Pampa del Tamarugal Basin throughout the Holocene. Average relative humidity estimates are within the error range of modern observed values. Increased variance in the relative humidity occurs between 4.9 ka and 1.8 ka. The lowest variance is observed at 7.7 ka during the Mid-Holocene decrease in El Niño frequency and intensity. B) Calculated box-plot showing range of intrinsic water-use efficiency over the Holocene period. Values increase gradually over the study period and periods with lower iWUE are interpreted as intervals during which water availability is greater. Number of individual ring measurements (n) for each interval provided below each box (these values are the same for RH estimates).

correlation follows current understanding of the iWUE parameter (Frank et al., 2015), with increasingly arid conditions in the PdT resulting in an increase in iWUE and plant water conservation. In addition to the rising atmospheric aridity, groundwater availability in the PdT has decreased substantially over the modern period. Aggressive extraction of water for human use has lowered groundwater as much as 20 m in some parts of the PdT basin (Chavez et al., 2016). Both atmospheric CO_2 and water availability can influence the iWUE; therefore, both atm. CO_2 and RH are used in tandem in order to interpret the paleo-climate record within the tree series.

In summary, increased RH and decreased iWUE indicate a humid period; a decrease in RH and an increase in iWUE represent a dry period. When these two parameters do not display this inverse relationship, interpretation is aided by comparison with other climate records or is attributed to unidentifiable environmental drivers (e.g. insect infestation, fires, etc).

4.2. Ancient *Prosopis sp.* record

The ancient *Prosopis* sp. isotope timeseries indicate that the Atacama experienced climatic changes that are consistent with the hypothesis that high Andean precipitation was the dominant source of groundwater recharge to the PdT over the Holocene period. The primary evidence for this comes from comparison between the *Prosopis* sp. $\delta^{18}O$ and Sajama ice core $\delta^{18}O$ data (Thompson et al., 1998). The mean values of the individual ^{14}C-dated tree-ring series and the overlapping coarser resolution ice core $\delta^{18}O$ data are highly correlated (r = 0.96, p < 0.001, n = 13). The variance between the overlapping Sajama and *Prosopis* sp. $\delta^{18}O$ datasets is also significantly correlated (r = 0.75, p = 0.002, n = 13) (Fig. 9A). The tree-ring variance is consistently greater than that observed in the ice core record. This result is expected given the higher-resolution tree-ring data inherently captures more variability. Despite the isotopic fractionation that occurs due to the variable contribution for evaporative leaf waters, the $\delta^{18}O$ value of groundwater used by *Prosopis* sp. is clearly retained in the average $\delta^{18}O$ values of the tree-ring α–cellulose. Three samples from archaeological sites of Ramaditas and Caserones (see Table 2) were excluded from this comparison based on their relationship to the archaeological sites. It is likely that these samples received at least some water from irrigation at the sites; therefore, they represent human modification of the landscape that might conflate the climate signal (see section 4.2.3).

Changes in the average $\delta^{18}O$ values between sample periods is not likely attributed to regional differences in groundwater $\delta^{18}O$ values between the four sample sites. The Ramaditas, Guatacondo, and Llamara sites are all located along the Quebrada Guatacondo. The $\delta^{18}O$ value of modern groundwater samples from the upper drainage ~2000 masl ($\delta^{18}O = -5.7$ $\sigma = 0.7$) is very similar to values in the lower portion of the drainage ~800 masl ($\delta^{18}O = -7.1$ $\sigma = 0.3$). Taking into account the +1.4‰ difference in modern $\delta^{18}O$ groundwater values from this drainage and considering only paleo-tree samples from the Guatacondo drainage, the trend in mean $\delta^{18}O$ α–cellulose values observed over the Holocene remains the same. Therefore, the agreement between the oxygen isotope values of the tree-ring and ice core records is due to changes in the isotopic value of Andean precipitation.

The $\delta^{18}O_{ac}$ record presented here reflects changes in the isotope value of high Andean precipitation which recharges groundwater in the PdT basin. Changes in the oxygen isotope value of precipitation ($\delta^{18}O_{precip}$) in the Andes has been attributed to variability in atmospheric circulation or modes that alter the degree of rain-out or transport efficiency of the South American summer monsoon (SASM) (Vuille et al., 2012). For the arid south-central Andes to the east of the Atacama, precipitation is highly seasonal with upwards of 70% of annual rainfall occurring between December and February this austral summer; this precipitation originates over the tropical Atlantic Ocean and flows along the easterlies (Garreaud et al., 2003). Since precipitation only occurs during the SASM, changes in moisture source

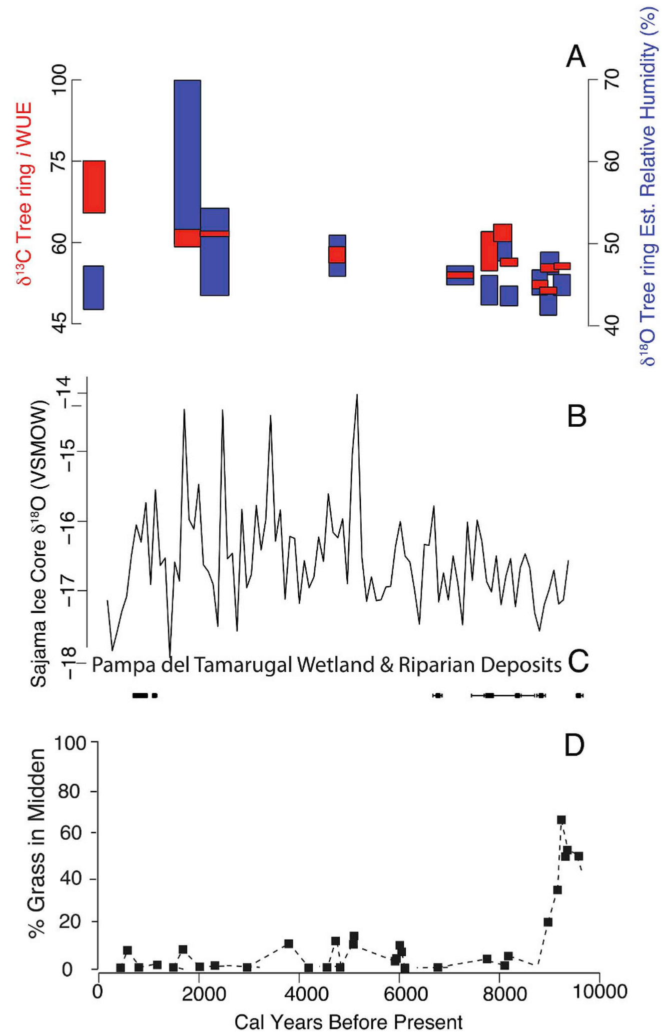

Fig. 9. Comparison of ancient *Prosopis* sp. $\delta^{18}O$ relative humidity and $\delta^{13}C$ intrinsic water-use efficiency (iWUE) records (a) from the PdT, the Sajama ice core $\delta^{18}O$ record (b) (Thompson et al., 1998). Paleowetland data (c) of groundwater table depth from the PdT (c; Pfieffer et al., 2018a,b). Rodent midden grass point count abundance (d; Latorre et al., 2002, 2003), showing previously classified wet periods.

(associated with anomalous events) in this region have a minimal effect on isotope values (Vuille et al., 2003a). Modern observation of conditions at the Sajama ice cap, in the Bolivian high Andes (18° S), show that the $\delta^{18}O_{ice}$ record recovered by Thompson et al. (1998) is strongly related to precipitation amount and accumulation; these two factors explain half the variance observed during the modern period (Hardy et al., 2003). Previously the Sajama $\delta^{18}O_{ice}$ record was interpreted as a record of changes in temperature spanning the last 25,000 years (Thompson et al., 1998). However, this interpretation disagrees with observational, modeling, and other paleoclimate proxy studies (Vuille et al., 2003b; Hardy et al., 2003; Vimeux et al., 2009; Bird et al., 2011; van Breukelen et al., 2008; Jomelli et al., 2011). The strength of SASM is linked to the position of the Intertropical Convergence Zone (ITCZ) and variability in mean-state conditions in the Atlantic and Pacific Oceans particularly with respect to temperature and precipitation (Zhou and Lau, 1998; Arz et al., 2001; Vuille and Werner, 2005; Vuille et al., 2012). For example, increased (decreased) sea surface temperatures (SST) in the Pacific during El Niño (La Niña) events increased (decrease) westerlies wind strength resulting in drier (wetter) conditions in the high Andes (eg. Vuille et al., 2000). Changes in Atlantic SST over the Holocene is linked to shifts in thermohaline circulation

(AMOC) intensity related to ice-rafted debris and freshwater pulses into the Atlantic (Bond et al., 1997; Carlson et al., 2008). Increased SASM is connected to reduced AMOC and increased Atlantic SST gradients (Strikis et al., 2011). These dynamics influencing SASM precipitation in the high Andes are the driving processes of variability in $\delta^{18}O_{precip}$. Shifts in atmospheric circulation and strength of the SASM are what drive these changes in the $\delta^{18}O_{precip}$ recharging the Atacama aquifers over the Holocene.

The obvious connection between the hydroclimate in the PdT and the Sajama ice core, from two distinct climatic zones, has important implicates for the identification of region shifts in water availability and its influence on ancient human cultures. Comparison of the tree-ring isotope derived RH estimates and iWUE values provide a more detailed history of hydroclimatic change and facilitates discussion in reference to other climate data sets over each of the discrete intervals in the *Prosopis* sp. record.

4.2.1. Early Holocene climate record

Prosopis sp. tree series date to a nearly continuous thousand-year period during the early Holocene (with series dating between 9.7 to 9.3 and 9.2 to 8.6 ka). These data indicate that conditions in the Atacama are wetter and less variable than modern conditions. The early Holocene tree-ring series agree in terms of variability and water availability with other paleoclimate proxies from the Atacama and larger Andean region.

During the interval from 9.7 to 9.3 ka isotope-based iWUE decreases while RH estimates are higher than modern indicating greater water availability. These support regional paleoclimate datasets including Atacama rodent middens (Betancourt et al., 2000; Latorre et al., 2006), wetland deposits (Quade et al., 2008; Pfieffer et al., 2018a,b), and higher lake levels in the Altiplano including at Lake Titicaca (Grosjean et al., 1997; Tapia et al., 2003). From 9.2 to 8.6 ka iWUE and RH increase, this unusual pattern occurs in the peak of the Holocene thermal maximum when increased westerly winds (Pearson and Palmer, 2000) may have blocked easterly flow effectively decreasing recharge to the PdT basin a phenomenon seen today (Houston, 2006) and in the past (e.g. Baker and Fritz, 2015). The decrease in recharge would have led to lowering of the groundwater table while strengthened westerly winds may have transported coastal fog farther inland to the PdT.

During this period ENSO activity was variability but not statistically different from the Late Holocene, as measured in mollusk aragonitic skeletons from the coast of Peru (Carré et al., 2014). However, the Pros*opis* sp. isotope records do not show increased interannual variance during the early Holocene window. One possible explanation for low variance in our record during this period is that increased water availability and higher groundwater levels during the early Holocene cause *Prosopis* sp. to be less sensitive to ENSO variance. Comparison with future high-resolution EP ENSO proxies over this interval may help elucidate these differences.

4.2.2. Middle Holocene

The mid–Holocene interval (8.6–4.9 ka) in the Atacama has been a period of debate among climate researchers for the past twenty years (Betancourt et al., 2000; Rech et al., 2002, 2003; Grosjean et al., 2003). Wetland deposits from the region have been interpreted as representative of humid conditions with high water tables (Betancourt et al., 2000), as well as, dry conditions with low flow conditions leading to accumulation of these deposits (Grosjean et al., 2003). Lacustrine records from this period indicate that while the mid-Holocene is drier than the early Holocene it is punctuated by humid intervals spanning decades to centuries (Grosjean et al., 1997). During this interval riparian flood deposits indicate that groundwater levels rose between 8.6 and 7.7 ka in response to pluvial events (Pfeiffer et al., 2018a,b). Despite these flood events the $\delta^{18}O$ *Prosopis* sp. record shows low variability as does the Sajama ice core $\delta^{18}O$ record (Thompson et al., 1998). Low interannual variability attributed to a reduction in ENSO variability is also seen in this period ~7 ka in a $\delta^{18}O$ stalagmite record from Peru (Chen et al., 2016). Pluvial events in the PdT sourced from high-altitude precipitation therefore resulted in consistent meteoric water $\delta^{18}O$ values, which are indistinguishable from the preceding period (the early Holocene).

The $\delta^{13}C$ *Prosopis* sp. data bracket a period of increased aridity for the region, between 8.4 and 8.3 ka, when iWUE is higher than samples from the early Holocene (9.6–8.6 ka) and the proceeding sample from 7.7 ka. The sub-annual $\delta^{13}C$ record from sample IGSN: IE18O000E dating to 8.3 ka has a similar seasonal trend to the modern dataset; however, the maximum intra-ring difference for 8.3 ka $\delta^{13}C$ is 1.7‰, which is 0.6‰ greater than the most extreme modern sample. The increase in the maximum difference of intra-ring $\delta^{13}C$ is attributed to greater inter-seasonal differences in temperature and RH. Enhanced coastal upwelling along the west coast of South America (15–18° S) during the mid–Holocene likely resulted in an increased influence of coastal fog on terrestrial ecosystems at mid–altitudes (Fontugne et al., 1999). Enhanced coastal fog and decreased Pacific sea surface temperatures, ~1 to 4 °C based on coastal mollusk $\delta^{18}O$ isotope records (Carré et al., 2011), coupled with increasing aridity in the high Andes to the east from 8.4 to 8.0 ka (Geyh et al., 2017) likely created the extreme interseasonal differences observed in our subring record. These climatic trends found in independent proxy records present conditions that are known to result in increased iWUE in *Prosopis* sp. (i.e. increased aridity and enhanced coastal fog). The *Prosopis* sp. $\delta^{18}O$ isotope record shows little change in the basin estimated decadal RH over this same interval and the increased coastal fog documented by Fontugne et al. (2004) perhaps is not detected in our annual sampling at 8.4–8.0 ka. Seasonal changes in fog occurrence have been observed in *Sequoia sempervirens* and future work on modern *Prosopis* sp. growing in coastal fog areas may find a similar signal (Roden et al., 2009).

Relative humidity increases slightly at 8.3 ka and at 7.7 ka there is a slight decrease in iWUE. Around 7.7 ka (IGSN: IE18O000C) the smallest range for RH and iWUE indicates that atmospheric conditions were likely less variable during this period. The low variability in the *Prosopis* sp. record coincides with a dry interval in South American climate between 8.3 and 7.8 ka identified via the titanium concentration within laminated sediment from the Caraico Basin core indicating maximum aridity at ~5.0 ka (Haug et al., 2001; Peterson and Haug, 2006). During this dry interval monsoonal precipitation was reduced. A decrease in mid–Holocene (7–5 ka) El Niño frequency and intensity due to orbital forcing (Clement et al., 2000) and the resultant southward shift of seasonal wind stress anomalies initiating suppression of the Eastern Pacific ENSO progression (Karamperidou et al., 2015) has been well documented (eg. Sandweiss et al., 2001; Shin et al., 2006). Alluvial sediments from the region suggest that during ENSO neutral conditions enhanced westerly flow and altered the hydrological regime of northern Chile resulting in more arid conditions from 8.6 to 5.7 ka (Ortega et al., 2012). The *Prosopis* sp. record suggest that the mid-Holocene suppression of ENSO ~7.7 ka led to decreased water availability in the hyperarid core of the Atacama Desert. The *Prosopis* sp. isotope records indicate that ~7.7 ka conditions in the Atacama Desert were less variable while series dating to ~8.3 and 4.9 ka ENSO–like variability is present. The timing of these changes in the *Prosopis* sp. record is synchronous with changes in the region previously attributed to ENSO variability.

4.2.3. Late Holocene cultural landscape

The greatest interannual variability in both $\delta^{18}O$ and $\delta^{13}C$ is observed in the late Holocene (2.5–1.8 ka) *Prosopis* sp. record. The late Holocene sediment records from 2 to 1 ka show increased ENSO activity resulting in wetter conditions (Rein et al., 2005; Moy et al., 2002; Thompson et al., 2017). Conversely, this increased variance is absent in high-resolution records over the same time period (Emile-Geay et al., 2016; Chen et al., 2016). The presence of increased variability in our high-resolution record is suggestive of ENSO influence, but attributing this variation to ENSO activity is premature and more rigorous statistical analysis on larger sample sizes is needed. Increased climatic variability in the late Holocene agrees with other proxy records, both locally and regionally; however, the *Prosopis* sp. $\delta^{13}C$ values indicate that the iWUE remain consistently high compared to other parts of the record. As a result, water availability likely remained low during the late Holocene, despite increased variability in other climate conditions.

It is important to note that an abundance of archaeological records from the region document the capacity of the human populations to alter their environment (Winterholder, 1980; Winterholder and Thomas, 1978; Dillehay and Kolata, 2004; Erickson, 2010; Nuñez et al., 2013). In the PdT region beginning as early as 3.5 ka human populations were farming former wetlands utilizing canal irrigation technology, artificial flooding of the landscape in this way could show up in the tree-ring isotope records as an artificial wet period (Adan et al., 2013; Gayo et al., 2012; Urbina Araya et al., 2012). As such, the anthropogenic influence on the *Prosopis* sp. isotope data and other proxy records must be considered. The question of climate change versus cultural landscape adaptation is difficult to ascertain and has been a subject of debate among Andean researchers (Kolata, 1986; Graffam et al., 1996; Erikson, 1999); the annual nature of our record allows us to evaluate this dichotomy on human timescales.

The late Holocene is a period of great cultural significance in the PdT as agricultural communities first appear and begin irrigating hundreds of hectares of land (Bryson, 2005; Maldonado et al., 2016). Some of the oldest evidence of copper metallurgy is seen in the PdT as early as 3.1 ka (Figueroa et al., 2015). Interregional trade networks appear to expand from the coast to the Andean highlands as evidenced by the resource remains at archaeological sites (Graffam et al., 1996; Rivera, 2008; Agüero, 2012). Changes in the scale of architecture ~2.4 ka lead to increasing use of tree trunks for building (Adán et al, 2007; Núñez and Santoro, 2011; Uribe, 2006) and is perhaps the first large-scale tree culling in the region's history (Gayo et al., 2019). Extensive agricultural development, settlement construction, and artisanal production during this period of cultural fluorescence marks the beginning of the Anthropocene in the PdT (Gayo et al., 2019) requiring increased scrutiny and consideration of human-influence on the tree-ring isotope record during the late Holocene.

The precise timing of when these cultures began to flourish is obscured by the use of ancient wood resources in the area. For example, a tree sample (IGSN: IE18O000E) dating to 4.9 ka comes from the plaza at the Guatacondo archaeological site, where other ^{14}C dates from organic materials (carbon, seeds, etc.) are limited to 2.3–1.8 ka. As with the samples collected in this study, the presence of wood thousands of years older than archaeological remains at the Guatacondo site exemplifies the old wood problem in this region, which has plagued archaeological investigations in the Andes for decades (for review see Kennett et al., 2002; Rademaker et al., 2013). Typologies of ceramics and architecture provide evidence for site occupation during this cultural interval (Rodriguez and Montero, 2012); the *Prosopis* sp. records lend credence to the antiquity of these sites. The use of ancient *Prosopis* sp. wood by ancient populations complicates the precise dating of the archaeological sites; however, by comparing the ^{14}C dates of structural wood beams and organic remains the period of occupation becomes apparent (Fig. 10). The integration of the ^{14}C dates from multiple materials at the sites along with the climate time series from the *Prosopis* sp tree-rings also allows for the interpretation of human-climate interactions over this important cultural period.

Extremes in RH estimates from trees sampled within the structures at the Ramaditas site date between 2.5 and 2.4 ka. We hypothesize that occupation at Ramaditas began ~2.4 ka based on the isotope record in sample IGSN: IE18O0001, which was found with its roots intact next to one of the structures at Ramaditas. The large downward spike in this record is the lowest raw $\delta^{18}O$ values from this period (~2.4 ka) and may be evidence for a flood event just prior to site occupation (proposed initial construction at Ramaditas). The demise of sample IGSN: IE18O0001 coincides with the first ^{14}C dates from archaeological deposits within the structure site supporting this hypothesis. During site occupation between 2.4 and 1.8 ka, high water availability is indicated in the *Prosopis* sp. record via lowered iWUE and higher mean RH. Greater water availability is also observed in other local climate records (Rech et al., 2003; Latorre et al., 2006, Fig. 9). Indeed, this wet interval is marked in other areas of the Andes and is attributed to increased ENSO variability (e.g. Thompson et al., 2003). At all three archaeological sites the data suggest that for a brief time ~1.9 ka water availability was higher, but this was followed by a period of increasing aridity up until the abandonment of the Guatacondo and Ramaditas sites circa ~1.8 ka. The abandonment of the Guatacondo and Ramaditas sites, therefore, may be related to increasing aridity while the occupants of the Caserones site were able to withstand this climatic change.

Variability in the $\delta^{18}O$ and $\delta^{13}C$ α–cellulose series record the decadal-scale humid events that led to the previous documentation of flood deposits in wetland records (Fig. 9C). Given the sub-decadal recurrence pattern of these wet periods we interpret them as possible ENSO-related flood events. While our proxy precludes the identification of flood events versus episodes of increase precipitation (i.e. wet periods) the presence of wetlands during this interval in the sedimentary record indicate that surface flooding did occur. The abrupt nature of these events likely caused massive destruction, as is seen at other archaeological sites in the Andes (Sandweiss et al., 2001). In this arid environment inconsistent intra-annual rainfall would have significantly challenged agricultural practices. While greater water availability, however intermittent, would have allowed cultures in the area to become agrarian (eg. Gayo et al., 2012; Marquet et al., 2012).

There is, however, one significant caveat with the *Prosopis* sp. samples collected from archaeological sites. While none of the samples collected in this study were recovered from directly irrigated fields, *Prosopis* sp. samples from 2.4 to 1.8 ka cannot be considered free of anthropogenic influence. It is possible, although unlikely in terms of scale, that periods of high RH and low iWUE identified in the isotope time series could reflect watering by humans via irrigation or silviculture practice. Given the agreement with other regional records from this time period, this interpretation is unlikely. Additionally, *Prosopis* sp. exude a toxin that would make them disadvantageous to other agricultural practices. Currently, *Schinus molle* trees are most commonly associated with agrarian practice, and future work on this species may provide better improve our ability to identify climatic versus anthropogenic signatures in tree–ring isotopes series.

5. Conclusions

The *Prosopis* sp. tree-ring isotope records provide the highest-resolution and longest temporally constant climate proxy from the Atacama Desert to date. The combined oxygen and carbon isotope approach facilitates a comprehensive assessment of Atacama hydroclimate variability over the Holocene. Most significantly, the correlation between the Sajama ice core $\delta^{18}O$ and average *Prosopis* sp. $\delta^{18}O$ values/variance indicate that groundwater recharge in the arid PdT Basin in the northern Atacama is driven primarily by precipitation in the high Andean Altiplano. Additionally, the decadal-scale variability in iWUE and RH recorded by the *Prosopis* sp. isotope data agree very well with other paleoclimate data from the region. Reconstructed iWUE values indicate that water availability is highest during the early Holocene when hydroclimate conditions were likely similar to the modern day. Middle Holocene records are complex, with higher than modern inter–seasonal variability ~8.3 ka and a decrease in variability likely due to changes in ENSO ~7.7 ka. Despite frequent flooding episodes during the Late Holocene, this is also a period when cultures developed large agricultural settlements in the PdT.

The results of this study also demonstrate that the *Prosopis* sp. records of wet/dry events in the PdT over the Holocene are sub-decadal in

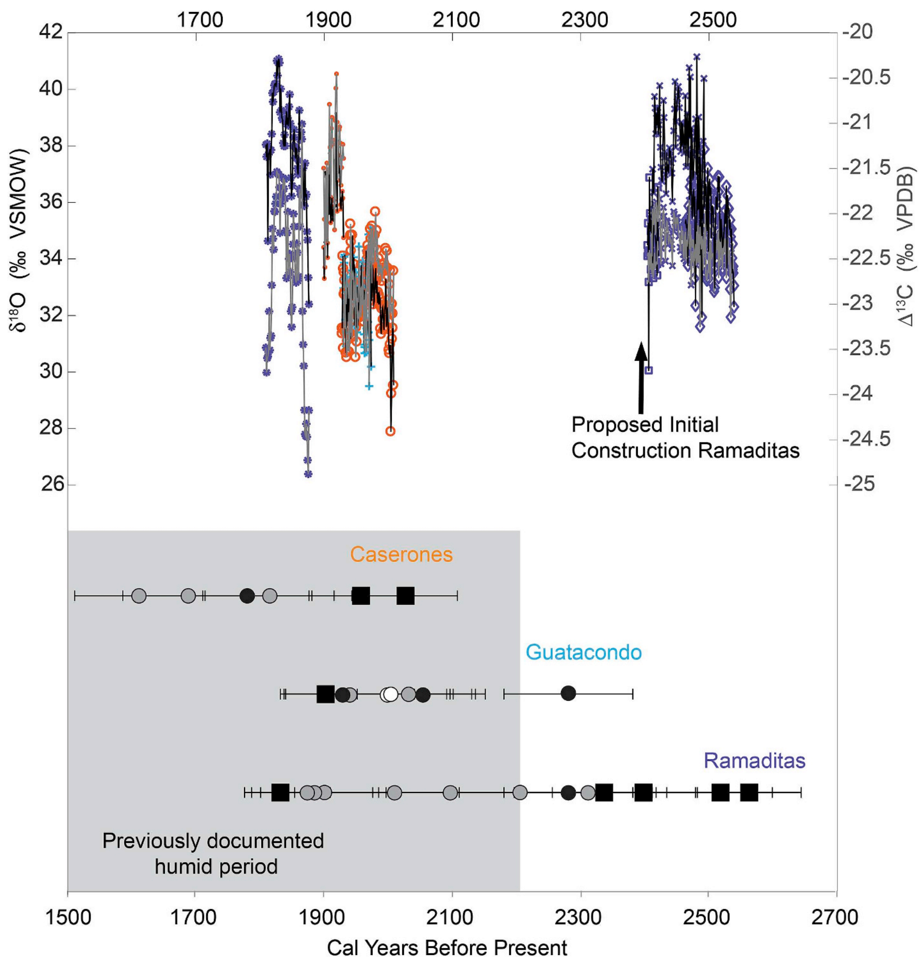

Fig. 10. Top graph ancient tree ring $\delta^{18}O$ and $\delta^{13}C$ records from archaeological sites. Individual trees have unique data point marker symbols with symbol color corresponding to the archaeological site of origin. Bottom graph shows ^{14}C dates for the archaeological sites from which wood was recovered for this study. The periods of occupation are delimited by ^{14}C-dated wood for which isotopic data was recovered (black squares), other wood dates (black circles), charcoal dates likely from wood (gray circles), and comestible macrobotanical dates (white circles).

nature and are likely regulated by ENSO variability. The sensitivity of the sub-annual modern tree-ring data, in addition to the similarity between the modern and ancient seasonal isotope signals indicate that future work on ring subsections from the ancient *Prosopis* sp. trees could provide additional insight into ENSO and SASM dynamics in the Atacama Desert. The *Prosopis* sp. isotope timeseries are particularly promising as a climate proxy since sub-decadal to seasonal datasets are necessary to resolve the primary modes of Holocene climate variability and improve future predictive capabilities.

Declaration of competing interest

There are no conflicts of interest to report.

Acknowledgments

Funding for this research was provided by a National Geographic Society Waitt Grant #W292–13 (Dodd), National Geographic Society Grants #7170–01, #8373–07, and #8836–10 (Rivera), Fondo de Ciencia y Tecnologia, Fondecyt–Chile Grants #1990003–799003 (Rivera), NEH Grant RK–20003–93 (Rivera), NIU College of Liberal Arts and Sciences Research and Artistry Grant (Dodd), Geological Society of America Student Research Grant (Olson), The Marie Morisawa Award from the Quaternary Geology and Geomorphology Division of the Geological Society of America (Olson), Lewis and Clark Grant from the American Philosophical Society (Olson), and a Tilford Field Studies Scholarship from the Association of Environmental and Engineering Geologists (Olson). We would like to thank Jorge Moya, Raquel Pinto, Dan Shea and the Beloit College Archeology Field School, Marco Castillo, Richard Jayne, Ryan Pollyea, Susan Swanson, and David Reid for field assistance. Aaron Dieffendorf and Erika Freimuth for leaf $\delta^{13}C$ analysis.

Appendix A. Supplementary data

Supplementary data to this article can be found online at https://doi.org/10.1016/j.palaeo.2019.109408.

References

Abbott, M.B., Wolfe, B.B., Wolfe, A.P., Seltzer, G.O., Aravena, R., Mark, B.G., et al., 2003. Holocene paleohydrology and glacial history of the central Andes using multiproxy lake sediment studies. Palaeogeogr. Palaeoclimatol. Palaeoecol. 194 (1–3), 123–138.

Aceituno, P., 1988. On the functioning of the Southern oscillation in the south American sector. Part I: surface climate. Mon. Weather Rev. 116 (3), 505–524. https://doi.org/10.1175/1520–0493(1988)116<0505:otfots>2.0.co;2.

Adán, L., Urbina, S., Uribe, M., 2007. Arquitectura pública y doméstica en las quebradas de Pica-Tarapacá: asentamiento y dinámica social en el Norte Grande de Chile (900–1450 DC). Procesos Sociales Prehispánicos en el Sur Andino. La vivienda, la comunidad y el territorio 183–206.

Adán, L., Urbina, S., Pellegrino, C., Agüero, C., 2013. Aldeas en los bosques de Prosopis: arquitectura residencial y congregacional en el período Formativo tarapaqueño (900 ac-900 DC). Estud. Atacameños 45, 75–94.

Agüero, C., 2012. Textiles del asentamiento Caserones y su cementerio: significado social y político para la población Tarapaqueña durante el período Formativo (Norte de Chile). Revista Chilena De Antropología 0 (26). https://doi.org/10.5354/0719–1472.

2012.26555.
Alpers, C.N., Whittemore, D.O., 1990. Hydrogeochemistry and stable isotopes of ground and surface waters fromtwo adjacent closed basins, Atacama Desert, northern Chile. Appl. Geochem. 5 (5–6), 719–734. https://doi.org/10.1016/0883–2927(90)90067–f.
Anchukaitis, K.J., Evans, M.N., Lange, T., Smith, D.R., Leavitt, S.W., Schrag, D.P., 2008. Consequences of a rapid cellulose extraction technique for oxygen isotope and radiocarbon analyses. Anal. Chem. 80 (6), 2035–2041.
Anderson, W.T., Bernasconi, S.M., McKenzie, J.A., Saurer, M., Schweingruber, F., 2002. Model evaluation for reconstructing the oxygen isotopic composition in precipitation from tree ring cellulose over the last century. Chem. Geol. 182 (2–4), 121–137.
Aravena, R., 1995. Isotope hydrology and geochemistry of northern Chile groundwaters. Bull. IFEA 24 (3), 495–503.
Aravena, R., Suzuki, O., 1990. Isotopic evolution of river water in the northern Chile region. Water Resour. Res. 26 (12), 2887–2895.
Arz, H.W., Gerhardt, S., Patzold, J., Rohl, U., 2001. Millennial-scale changes of surface- and deep-water flow in the western tropical Atlantic linked to Northern Hemisphere high-latitude climate during the Holocene. Geology 29 (3), 239–242.
Baker, P.A., Fritz, S.C., 2015. Nature and causes of Quaternary climate variation of tropical South America. Quat. Sci. Rev. 124, 31–47.
Baker, P.A., Seltzer, G.O., Fritz, S.C., Dunbar, R.B., Grove, M.J., Tapia, P.M., et al., 2001. The history of South American tropical precipitation for the past 25,000 years. Science 291 (5504), 640–643. https://doi.org/10.1126/science.291.5504.640.
Ballantyne, A.P., Rybczynski, N., Baker, P.A., Harington, C.R., White, D., 2006. Pliocene Arctic temperature constraints from the growth rings and isotopic composition of fossil larch. Palaeogeogr. Palaeoclimatol. Palaeoecol. 242 (3–4), 188–200. https://doi.org/10.1016/j.palaeo.2006.05.016.
Barbour, M.M., 2007. Stable oxygen isotope composition of plant tissue: a review. Funct. Plant Biol. 34 (2). https://doi.org/10.1071/FP06228. 83.
Bert, D., Leavitt, S.W., Dupouey, J.L., 1997. Variations of wood $\delta^{13}C$ and water-use efficiency of Abies alba during the last century. Ecology 78 (5). https://doi.org/10.2307/2266151. 1588.
Betancourt, J.L., Latorre, C., Rech, J.A., Quade, J., Rylander, K.A., 2000. A 22,000–year record of monsoonal precipitation from northern Chile's Atacama Desert. Science 289 (5484), 1542–1546. https://doi.org/10.1126/science.289.5484.1542.
Bird, B.W., Abbott, M.B., Rodbell, D.T., Vuille, M., 2011. Holocene tropical South American hydroclimate revealed from a decadally resolved lake sediment δ18O record. Earth Planet. Sci. Lett. 310 (3–4), 192–202.
Blanco, N., Tomlinson, A.J., 2013. Carta Guatacondo, Región de Tarapacá. Carta Geológica de Chile, Serie Geológica Básica, vol. 156.
Bond, G., Showers, W., Cheseby, M., Lotti, R., Almasi, P., Priore, P., et al., 1997. A pervasive millennial-scale cycle in North Atlantic Holocene and glacial climates. Science 278 (5341), 1257–1266.
Brendel, O., Iannetta, P.M., Stewart, D., 2000. A rapid and simple method to isolate pure alpha–cellulose. Phytochem. Anal. 11 (1), 7–10.
Van Breukelen, M.R., Vonhof, H.B., Hellstrom, J.C., Wester, W.C.G., Kroon, D., 2008. Fossil dripwater in stalagmites reveals Holocene temperature and rainfall variation in Amazonia. Earth Planet. Sci. Lett. 275 (1–2), 54–60.
Bryson, R.U., 2005. In: Arqueologia del Desierto de Atacama, M.A.Rivera (Ed.), Implications of Macrophysical Paleoclimatic Models for Irrigation Agriculture at Ramaditas. Editorial Universidad Bolivariana/LOM, Santiago, pp. 37–71 Northern Chile.
Calderon, G., Garrido, M., Acevedo, E., 2015. Prosopis tamarugo Phil.: a native tree from the Atacama Desert groundwater table depth thresholds for conservation. Rev. Chil. Hist. Nat. 88, 1–8.
Carlson, A.E., LeGrande, A.N., Oppo, D.W., Came, R.E., Schmidt, G.A., Anslow, F.S., Obbink, E.A., 2008. Rapid early Holocene deglaciation of the Laurentide ice sheet. Nat. Geosci. 1 (9), 620.
Carré, M., Azzoug, M., Bentaleb, I., Chase, B.M., Fontugne, M., Jackson, D., et al., 2011. Mid–Holocene mean climate in the south eastern Pacific and its influence on South America. Quat. Int. 112. https://doi.org/10.1016/j.quaint.2011.02.004.
Carré, M., Sachs, J.P., Purca, S., Schauer, A.J., Braconnot, P., Falcón, R.A., Julien, M., Lavallée, D., 2014. Holocene history of ENSO variance and asymmetry in the eastern tropical Pacific. Science 345 (6200), 1045–1048.
Cereceda, P., Osses, P., Larrain, H., Farıas, M., Lagos, M., 2002. Advective, orographic and radiation fog in the Tarapacá region, Chile. Atmos. Res. 64 (1–4), 261–271.
Cereceda, P., Larrain, H., Osses, P., Farías, M., Egaña, I., 2008. The spatial and temporal variability of fog and its relation to fog oases in the Atacama Desert, Chile. Atmos. Res. 87 (3–4), 312–323. https://doi.org/10.1016/j.atmosres.2007.11.012.
Cernusak, L.A., Wong, S.C., Farquhar, G.D., 2003. Oxygen isotope composition of phloem sap in relation to leaf water in Ricinus communis. Funct. Plant Biol. 30 (10), 1059–1070.
Chávez, R.O., Clevers, J.G.P.W., Herold, M., Ortiz, M., Acevedo, E., 2013. Modelling the spectral response of the desert tree Prosopis tamarugo to water stress. Int. J. Appl. Earth Obs. Geoinf. 21, 53–65.
Chávez, R.O., Clevers, J.G.P.W., Decuyper, M., De Bruin, S., Herold, M., 2016. 50 years of water extraction in the Pampa del Tamarugal basin: can *Prosopis tamarugo* trees survive in the hyper-arid Atacama Desert (Northern Chile)? J. Arid Environ. 124, 292–303.
Chen, S., Hoffmann, S.S., Lund, D.C., Cobb, K.M., Emile-Geay, J., Adkins, J.F., 2016. A high-resolution speleothem record of western equatorial Pacific rainfall: implications for Holocene ENSO evolution. Earth Planet. Sci. Lett. 442, 61–71.
Clement, A., Seager, R., Cane, M., 2000. Suppression of el Niño during the mid–Holocene by changes in the earth's orbit. Paleoceanography 15 (6), 731–737.
Csank, A.Z., Fortier, D., Leavitt, S.W., 2013. Annually resolved temperature reconstructions from a late Pliocene–early Pleistocene polar forest on Bylot Island, Canada. Palaeogeogr. Palaeoclimatol. Palaeoecol. 369, 313–322.
Dansgaard, W., 1964. Stable isotopes in precipitation. Tellus 16 (4), 436–468.
Dillehay, T., Kolata, A., 2004. Long-term human response to uncertain environmental conditions in the Andes. Proc. Natl. Acad. Sci. 101 (12), 4325–4330.
Dodd, J.P., Patterson, W.P., Holmden, C., Brasseur, J.M., 2008. Robotic micromilling of tree-rings: a new tool for obtaining subseasonal environmental isotope records. Chem. Geol. 252 (1–2), 21–30.
Duquesnay, A., Breda, N., Stievenard, M., Dupouey, J.L., 1998. Changes of tree–ring $\delta^{13}C$ and water–use efficiency of beech (Fagus sylvatica L.) in north–eastern France during the past century. Plant, Cell Environ. 21 (6), 565–572. https://doi.org/10.1046/j.1365–3040.1998.00304.x.
Ehleringer, J.R., 1993. Carbon and water relations in desert plants: an isotopic perspective. Stable isotopes. Plant Carbon–Water Relations 155–172.
Elsig, J., Schmitt, J., Leuenberger, D., Schneider, R., Eyer, M., Leuenberger, M., et al., 2009. Stable isotope constraints on Holocene carbon cycle changes from an Antarctic ice core. Nature 461 (7263), 507–510. https://doi.org/10.1038/nature08393.
Emile-Geay, J., Cobb, K.M., Carré, M., Braconnot, P., Leloup, J., Zhou, Y., Harrison, S.P., Correge, T., McGregor, H.V., Collins, M., Driscoll, R., 2016. Links between tropical Pacific seasonal, interannual and orbital variability during the Holocene. Nat. Geosci. 9 (2) 168.
Erickson, C.L., 1999. Neo–environmental determinism and agrarian “collapse”in Andean prehistory. Antiquity 73 (281), 634–642.
Erickson, C., 2010. The transformation of environment into landscape: the historical ecology of monumental earthwork construction in the Bolivian Amazon. Diversity 2, 618–652.
Evans, M.N., Schrag, D.P., 2004. A stable isotope–based approach to tropical dendroclimatology. Geochem. Cosmochim. Acta 68 (16), 3295–3305. https://doi.org/10.1016/j.gca.2004.01.006.
Ewing, S.A., Sutter, B., Owen, J., Nishiizumi, K., Sharp, W., Cliff, S.S., Perry, K., Dietrich, W., McKay, C.P., Amundson, R., 2006. A threshold in soil formation at Earth's arid–hyperarid transition. Geochem. Cosmochim. Acta 70 (21), 5293–5322.
Farquhar, G.D., Richards, R.A., 1984. Isotopic composition of plant carbon correlates with water–use efficiency of wheat genotypes. Funct. Plant Biol. 11 (6), 539–552.
Feng, X., 1999. Trends in intrinsic water–use efficiency of natural trees for the past 100–200 years: a response to atmospheric CO2 concentration. Geochem. Cosmochim. Acta 63 (13–14), 1891–1903. https://doi.org/10.1016/S0016–7037(99)00088–5.
Fichtler, E., Helle, G., Worbes, M., 2010. Stable–carbon isotope time series from tropical tree rings indicate a precipitation signal. Tree-Ring Res. 66 (1), 35–49. https://doi.org/10.3959/2008–20.1.
Figueroa, V., Salazar, D., Mille, B., Manríquez, G., 2015. Metal use and production among coastal societies of the Atacama Desert. Archaeometry 57 (4), 687–703.
Flinn, R.C., Archer, S., Boutton, T.W., Harlan, T., 1994. Identification of annual rings in an arid–land woody Plant,Prosopis glandulosa. Ecology 75 (3), 850–853. https://doi.org/10.2307/1941741.
Fontugne, M., Usselmann, P., Lavallee, D., Julien, M., Hatte, C., 1999. El Niño variability in the coastal desert of southern Peru during the mid–Holocene. Quat. Res. 52 (2), 171–179.
Fontugne, M., Carré, M., Bentaleb, I., Julien, M., Lavallée, D., 2004. Radiocarbon reservoir age variations in the South Peruvian upwelling during the Holocene. Radiocarbon 46 (02), 531–537. https://doi.org/10.1017/s003382220003558x.
Francey, R.J., Allison, C.E., Etheridge, D.M., Trudinger, C.M., Enting, I.G., Leuenberger, M., et al., 1999. A 1000-yearhigh precision record of $\delta^{13}C$ in atmospheric CO_2. Tellus B 51 (2), 170–193.
Frank, D.C., Poulter, B., Saurer, M., Esper, J., Huntingford, C., Helle, G., et al., 2015. Water-use efficiency and transpiration across European forests during the Anthropocene. Nat. Clim. Chang. 5 (6), 579.
Fritz, P., Suzuki, O., Silva, C., Salati, E., 1981. Isotope hydrology of groundwaters in the Pampa del Tamarugal, Chile. J. Hydrol. 53 (1), 161–184.
Frumkin, A., 2009. Stable isotopes of a subfossil *Tamarix* tree from the Dead Sea region, Israel, and their implications for the Intermediate Bronze Age environmental crisis. Quat. Res. 71 (3), 319–328. https://doi.org/10.1016/j.yqres.2009.01.009.
Garreaud, R., 2000. Intraseasonal variability of moisture and rainfall over the South American Altiplano. Mon. Weather Rev. 128 (9), 3337–3346.
Garreaud, R., Vuille, M., Clement, A.C., 2003. The climate of the Altiplano: observed current conditions and mechanisms of past changes. Palaeogeogr. Palaeoclimatol. Palaeoecol. 194 (1–3), 5–22.
Gayo, E.M., Latorre, C., Jordan, T.E., Nester, P.L., Estay, S.A., Ojeda, K.F., Santoro, C.M., 2012. Late Quaternary hydrological and ecological changes in the hyperarid core of the northern Atacama Desert (~21 °S). Earth Sci. Rev. 113 (3–4), 120–140. https://doi.org/10.1016/j.earscirev.2012.04.003.
Gayo, E.M., McRostie, V.B., Campbell, R., Flores, C., Maldonado, A., Uribe-Rodriguez, M., Moreno, P.I., Santoro, C.M., Christie, D.A., Muñoz, A.A., Gallardo, L., 2019. Geohistorical records of the Anthropocene in Chile. Elem Sci Anth 7 (1), 15. https://doi.org/10.1525/elementa.353.
Geyh, M.A., Grosjean, M., Núñez, L., Schotterer, U., 2017. Radiocarbon reservoir effect and the timing of the late–glacial/early Holocene humid phase in the Atacama Desert (northern Chile). Quat. Res. 52 (02), 143–153.
Gomes, A.V., Bolzon de Muniz, G.I., 1988. Wood structure and ultrastructure of Prosopis Caldenia, P. chilensis and P.Juliflora and influence of ecological factors. In: Presented at the International Conference on Prosopis, vol. 2. Recife, Brazil, pp. 25–29 Aug 1986.
Graffam, G., Rivera, M., Carevič, A., 1996. Ancient metallurgy in the atacama: evidence for copper smelting during Chile's Early Ceramic Period. Lat. Am. Antiq. 7 (2), 101–113.
Grosjean, M., 2001a. A 22,000 14C year BP sediment and pollen record of climate change from Laguna Miscanti(23°S), northern Chile. Glob. Planet. Chang. 28 (1–4), 35–51. https://doi.org/10.1016/s0921–8181(00)00063–1.

Grosjean, M., 2001b. Mid–holocene climate in the south–central Andes: humid or dry? Science 292 (5526). https://doi.org/10.1126/science.292.5526.2391a. 2391a–2391.
Grosjean, M., Núñez, L., Cartajena, I., Messerli, B., 1997. Mid–Holocene climate and culture change in the Atacama Desert, northern Chile. Quat. Res. 48 (02), 239–246. https://doi.org/10.1006/qres.1997.1917.
Grosjean, M., Cartajena, I., Geyh, M.A., Núñez, L., 2003. From proxy data to paleoclimate interpretation: the mid–Holocene paradox of the Atacama Desert, northern Chile. Palaeogeogr. Palaeoclimatol. Palaeoecol. 194 (1), ,247–258.
Hardy, D.R., Vuille, M., Bradley, R.S., 2003. Variability of snow accumulation and isotopic composition on Nevado Sajama, Bolivia. J. Geophys. Res.: Atmosphere 108 (D22).
Hartley, A., 2003. Andean uplift and climate change. Journal of the Geological Society 160 (1), 7–10 In press.
Haug, G.H., Hughen, K.A., Sigman, D.M., Peterson, L.C., Röhl, U., 2001. Southward migration of the intertropical convergence zone through the Holocene. Science 293 (5533), 1304–1308.
Helliker, B.R., Richter, S.L., 2008. Subtropical to boreal convergence of tree–leaf temperatures. Nature 454 (7203), ,511–514. https://doi.org/10.1038/nature07031.
Hogg, A.G., Hua, Q., Blackwell, P.G., Niu, M., Buck, C., Guilderson, T., et al., 2013. SHCAL13 southern Hemisphere calibration, 0–50,000 year cal BP. Radiocarbon 55 (2), 1–15.
Hook, B., Halfar, J., Gedalof, Z., Bollmann, J., 2013. Controlled breaking of mummified wood for use in paleoenvironmental analysis. Tree-Ring Res. 69 (2), 87–92. https://doi.org/10.3959/1536–1098–69.2.87.
Hook, B.A., Halfar, J., Gedalof, Z., Bollmann, J., Schulze, D., 2014. Stable isotope paleoclimatology of the earliest Eocene using kimberlite–hosted mummified wood from the Canadian Subarctic. Biogeosci. Discuss. 11 (11), 16269–16308. https://doi.org/10.5194/bgd–11–16269–2014.
Houston, J., 2006. Variability of precipitation in the Atacama Desert: its causes and hydrological impact. Int. J. Climatol. 26 (15), 2181–2198. https://doi.org/10.1002/joc.1359.
Houston, J., Hartley, A., 2003. The central Andean west-slope rainshadow and its potential contribution to the origin of hyper-aridity in the Atacama Desert. International Journal of Climatology: A Journal of the Royal Meteorological Society 23 (12), 1453–1464 In press.
Jahren, A.H., Sternberg, L., 2003. Humidity estimate for the middle Eocene Arctic rain forest. Geology 31 (5), 463.
Jahren, A.H., Sternberg, L.S.L., 2008. Annual patterns within tree rings of the Arctic middle Eocene (ca. 45 Ma): isotopic signatures of precipitation, relative humidity, and deciduousness. Geology 36 (2). https://doi.org/10.1130/G23876A.1. 99–4.
Jayne, R.S., Pollyea, R.M., Dodd, J.P., Olson, E.J., Swanson, S.K., 2016. Spatial and temporal constraints on regional–scale groundwater flow in the Pampa del Tamarugal Basin, Atacama Desert, Chile. Hydrogeol. J. 24, 1921–1937.
Jomelli, V., Khodri, M., Favier, V., Brunstein, D., Ledru, M.P., Wagnon, P., Blard, P.H., Sicart, J.E., Braucher, R., Grancher, D., Bourles, D.L., 2011. Irregular tropical glacier retreat over the Holocene epoch driven by progressive warming. Nature 474 (7350) 196.
Jordan, T.E., Kirk-Lawlor, N.E., Blanco, N.P., Rech, J.A., Cosentino, N.J., 2014. Landscape modification in response to repeated onset of hyperarid paleoclimate states since 14 Ma, Atacama Desert, Chile. GSA Bull. 126 (7–8), 1016–1046.
Karamperidou, C., Nezio, Di, Timmermann, P.N.A., Jin, F.F., Cobb, K.M., 2015. The response of ENSO flavors to mid-Holocene climate: implications for proxy interpretation. Paleoceanography 30 (5), 527–547.
Kennett, D.J., Ingram, B.L., Southon, J.R., Wise, K., 2002. Differences in 14C age between stratigraphically associated charcoal and marine shell from the archaic period site of kilometer 4, southern Peru: old wood or old water? Radiocarbon 44 (01), 53–58. https://doi.org/10.1017/s0033822200064663.
Kolata, A.L., 1986. The agricultural foundations of the Tiwanaku state: a view from the heartland. Am. Antiq. 51 (4), 748–762.
Krottenthaler, S., Pitsch, P., Helle, G., Locosselli, G.M., Ceccantini, G., Altman, J., et al., 2015. A power-driven increment borer for sampling high-density tropical wood. Dendrochronologia 36 (C), 40–44. https://doi.org/10.1016/j.dendro.2015.08.005.
Latorre, C., Betancourt, J.L., Rylander, K.A., Quade, J., 2002. Vegetation invasions into absolute desert: a 45000 yr rodent midden record from the Calama–Salar de Atacama basins, northern Chile (lat 22°–24° S). Geol. Soc. Am. Bull. 114 (3), 349–366.
Latorre, C., Betancourt, J.L., Rylander, K.A., Quade, J., Matthei, O., 2003. A vegetation history from the arid prepuna of northern Chile (22–23°S) over the last 13 500 years. Palaeogeogr. Palaeoclimatol. Palaeoecol. 194 (1–3), 223–246. https://doi.org/10.1016/S0031–0182(03)00279–7.
Latorre, C., Betancourt, J.L., Arroyo, M.T.K., 2006. Late Quaternary vegetation and climate history of a perennial river canyon in the Río Salado basin (22 S) of Northern Chile. Quat. Res. 65 (3), 450–466.
Latorre, C., Santoro, C.M., Ugalde, P.C., Gayo, E.M., Osorio, D., Salas-Egaña, C., Rech, J.A., 2013. Late Pleistocene human occupation of the hyperarid core in the Atacama Desert, northern Chile. Quat. Sci. Rev. 77, 19–30.
Leavitt, S., 2012. US Southwest monsoon precipitation inferred from tree-ring stable-carbon isotopes. Quat. Int. 279–280 269-270.
Leavitt, S.W., Idso, S.B., Kimball, B.A., Burns, J.M., Sinha, A., Stott, L., 2003. The effect of long-term atmospheric CO2 enrichment on the intrinsic water-use efficiency of sour orange trees. Chemosphere 50 (2), 217–222.
Linares, J.–C., Delgado–Huertas, A., Julio Camarero, J., Merino, J., Carreira, J.A., 2009. Competition and drought limit the response of water–use efficiency to rising atmospheric carbon dioxide in the Mediterranean fir Abies pinsapo. Oecologia 161 (3), 611–624. https://doi.org/10.1007/s00442–009–1409–7.
Lipp, J., Trimborn, P., Edwards, T., Waisel, Y., Yakir, D., 1996. Climatic effects on the $\delta^{18}O$ and $\delta^{13}C$ of cellulose in the desert tree Tamarix jordanis. Geochem. Cosmochim. Acta 60 (17), 3305–3309.
López, B.C., Sabaté, S., Gracia, C.A., Rodríguez, R., 2005. Wood anatomy, description of annual rings, and responses to ENSO events of Prosopis pallida H.B.K., a wide–spread woody plant of arid and semi–arid lands of Latin America. J. Arid Environ. 61 (4), 541–554. https://doi.org/10.1016/j.jaridenv.2004.10.008.
Majoube, M., 1971. Oxygen–18 and deuterium fractionation between water and steam (in French). J. Chim. Phys. Phys. Chim. Biol. 68, 1423–1436.
Maldonado, A., Santoro, C.M., Escallonia members, 2016. Climate change and social complexity in the Atacama Desert during the late quaternary. PAGES Magazine 24 (2), 56–57.
Margaritz, M., Aravena, R., Pena, H., Suzuki, O., Grilli, A., 1989. Water chemistry and isotope study of streams and springs in northern Chile. J. Hydrol. 108, 323–341.
Margaritz, M., Aravena, R., Pena, H., Suzuki, O., Grilli, A., 1990. Water chemistry and isotope study of streams and springs in northern Chile. J. Hydrol. 108, 323–341.
Marquet, P.A., Santoro, C.M., Latorre, C., Standen, V.G., Abades, S.R., Rivadeneira, M.M., et al., 2012. Emergence of social complexity among coastal hunter-gatherers in the Atacama Desert of northern Chile. Proc. Natl. Acad. Sci. 109 (37), 14754–14760.
Maseyk, K., Hemming, D., Angert, A., Leavitt, S.W., Yakir, D., 2011. Increase in water–use efficiency and underlying processes in pine forests across a precipitation gradient in the dry Mediterranean region over the past 30 years. Oecologia 167 (2), 573–585. https://doi.org/10.1007/s00442–011–2010–4.
McCarroll, D., Loader, N.J., 2004. Stable isotopes in tree rings. Quat. Sci. Rev. 23 (7–8), 771–801. https://doi.org/10.1016/j.quascirev.2003.06.017.
McCarroll, D., Pawellek, F., 1998. Stable carbon isotope ratios of latewood cellulose in Pinus sylvestris from northern Finland: variability and signal-strength. Holocene 8 (6), 675–684.
McCarroll, D., Gagen, M.H., Loader, N.J., Robertson, I., Anchukaitis, K.J., Los, S., et al., 2009. Correction of tree ringstable carbon isotope chronologies for changes in the carbon dioxide content of the atmosphere. Geochem. Cosmochim. Acta 73 (6), 1539–1547. https://doi.org/10.1016/j.gca.2008.11.041.
Messerli, B., Grosjean, M., Bonani, G., Bürgi, A., 1993. Climate change and natural resource dynamics of the Atacama Altiplano during the last 18,000 years: a preliminary synthesis. Mt. Res. 13 (2). https://doi.org/10.2307/3673629. 117.
Mooney, H.A., Gulmon, S.L., Rundel, P.W., Ehleringer, J., 1980. Further observations on the water relations of *Prosopos tamarugo* of the northern Atacama Desert. Oecologia 44, 177–180.
Moy, C.M., Seltzer, G.O., Rodbell, D.T., Anderson, D.M., 2002. Variability of el Niño/southern oscillation activity at millennial timescales during the Holocene epoch. Nature 420 (6912), 162.
Nester, P.L., Gayo, E., Latorre, C., Jordan, T.E., Blanco, N., 2007. Perennial stream discharge in the hyperarid Atacama Desert of northern Chile during the latest Pleistocene. Proc. Natl. Acad. Sci. 104, 19724–19729.
Núñez, L., 2002. Human occupations and climate change in the Puna de Atacama, Chile. Science 298 (5594), 821–824. https://doi.org/10.1126/science.1076449.
Núñez, L., Santoro, C.M., 2011. El tránsito arcaico-formativo en la circumpuna y valles occidentales del centro sur andino: hacia los cambios" neolíticos". Chungará 43, 487–530 ESPECIAL.
Núñez, L., Cartajena, I., Grosjean, M., 2013. Archaeological silence and ecorefuges: arid events in the Puna of atacama during the middle Holocene. Quat. Int. 307, 5–13.
Ortega, C., Vargas, G., Rutllant, J.A., Jackson, D., Méndez, C., 2012. Major hydrological regime change along the semiarid western coast of South America during the early Holocene. Quat. Res. 78 (03), 513–527. https://doi.org/10.1016/j.yqres.2012.08.002.
Pauly, M., Helle, G., Miramont, C., Büntgen, U., Treydte, K., Reinig, F., Guibal, F., Sivan, O., Heinrich, I., Riedel, F., Kromer, B., 2018. Subfossil trees suggest enhanced Mediterranean hydroclimate variability at the onset of the Younger Dryas. Sci. Rep. 8 (1) p.13980.
Pearson, P.N., Palmer, M., 2000. Atmospheric carbon dioxide concentrations over the past 60 million years. Nature 406, 695–699.
Peterson, L.C., Haug, G.H., 2006. Variability in the mean latitude of the Atlantic intertropical convergence zone as recorded by riverine input of sediments to the Cariaco basin (Venezuela). Palaeogeogr. Palaeoclimatol. Palaeoecol. 234 (1), 97–113. https://doi.org/10.1016/j.palaeo.2005.10.021.
Pfeiffer, M., Latorre, C., Gayo, E., Amundson, R., 2019. Rare calcium chloride–rich soil and implications for the existence of liquid water in a hyperarid environment. Geology 47 (2), 163–166 In press.
Pfeiffer, M., Latorre, C., Santoro, C.M., Gayo, E.M., Rojas, R., Carrevedo, M.L., McRostie, V.M., 2018a. Chronology, stratigraphy and hydrological modelling of extensive wetlands and paleolakes in the hyperarid core of the Atacama Desert during the late quaternary. Quat. Sci. Rev. 197, 224–245.
Pfeiffer, M., Latorre, C., Santoro, C.M., Gayo, E.M., Rojas, R., Carrevedo, M.L., McRostie, V.B., Finstad, K.M., Heimsath, A., Jungers, M.C., De Pol-Holz, R., 2018b. Chronology, stratigraphy and hydrological modelling of extensive wetlands and paleolakes in the hyperarid core of the Atacama Desert during the late quaternary. Quat. Sci. Rev. 197, 224–245.
De Porras, M.E., Maldonado, A., De Pol-Holz, R., Latorre, C., Betancourt, J.L., 2017. Late Quaternary environmental dynamics in the Atacama Desert reconstructed from rodent midden pollen records. J. Quat. Sci. 32 (6), 665–684.
Poussart, P.F., Evans, M.N., Schrag, D.P., 2004. Resolving seasonality in tropical trees: multi–decade, high–resolution oxygen and carbon isotope records from Indonesia and Thailand. Earth Planet. Sci. Lett. 218 (3–4), 301–316. https://doi.org/10.1016/S0012–821X(03)00638–1.
Quade, J., Rech, J.A., Betancourt, J.L., Latorre, C., Quade, B., Rylander, K.A., Fisher, T., 2008. Paleowetlands and regional climate change in the central Atacama Desert, northern Chile. Quat. Res. 69 (3), 343–360. https://doi.org/10.1016/j.yqres.2008.01.003.

Rademaker, K., Bromley, G.R.M., Sandweiss, D.H., 2013. Peru archaeological radiocarbon database, 13,000–7000 14C B.P. Quat. Int. 301, 34–45. https://doi.org/10.1016/j.quaint.2012.08.2052.

Ramsey, C.B., van der Plicht, J., Weninger, B., 2001. 'Wiggle matching'radiocarbon dates. Radiocarbon 43 (2A), 381–389.

Rech, J.A., Quade, J., Betancourt, J.L., 2002. Late quaternary paleohydrology of the central Atacama Desert (lat22–24 S), Chile. Geol. Soc. Am. Bull. 114 (3), 334–348.

Rech, J., Pigati, J., Quade, J., Betancourt, J., 2003. Re–evaluation of mid–Holocene deposits at Quebrada Puripica, northern Chile. Palaeogeogr. Palaeoclimatol. Palaeoecol. 194 (1–3), 207–222.

Rein, B., Lückge, A., Reinhardt, L., Sirocko, F., Wolf, A., Dullo, W.C., 2005. El Niño variability off Peru during the last 20,000 years. Paleoceanography 20 (4).

Rivera, M.A., 2008. The archaeology of northern Chile. The Handbook of South American Archaeology. pp. 963–977.

Robertson, I., Switsur, V.R., Carter, A.H.C., Barker, A.C., Waterhouse, J.S., Briffa, K.R., Jones, P.D., 1997a. Signal strength and climate relationships in 13C/12C ratios of tree ring cellulose from oak in east England. J. Geophys. Res.: Atmosphere 102 (D16), 19507–19516.

Robertson, I., Rolfe, J., Switsur, V.R., Carter, A.H.C., Hall, M.A., Barker, A.C., Waterhouse, J.S., 1997b. Signal strength and climate relationships in 13C/12C ratios of tree ring cellulose from oak in southwest Finland. Geophys. Res. Lett. 24 (12), 1487–1490.

Roden, J.S., Farquhar, G.D., 2012. A controlled test of the dual–isotope approach for the interpretation of stable carbon and oxygen isotope ratio variation in tree rings. Tree Physiol. 32 (4), 490–503. https://doi.org/10.1093/treephys/tps019.

Roden, J., Lin, G., Ehleringer, J., 1999. A mechanistic model for interpretation of hydrogen and oxygen isotope ratios in tree–ring cellulose. Geochem. Cosmochim. Acta 64 (1), 21–35.

Roden, J.S., Johnstone, J.A., Dawson, T.E., 2009. Intra–annual variation in the stable oxygen and carbon isotope ratios of cellulose in tree rings of coast redwood (Sequoia sempervirens). Holocene 19 (2), 189–197. https://doi.org/10.1177/0959683608098959.

Rodríguez, M.U., Montero, E.V., 2012. Sobre la secuencia cerámica del período Formativo de Tarapacá (900 ac–900dC): estudios en Pircas, Caserones, Guatacondo y Ramaditas, norte de Chile. Chungará 44 (2), 209–245. https://doi.org/10.4067/s0717–73562012000200003.

Sáez, A., Godfrey, L.V., Herrera, C., Chong, G., Pueyo, J.J., 2016. Timing of wet episodes in Atacama Desert over the last 15 ka. The groundwater discharge deposits (GWD) from Domeyko range at 25° S. Quat. Sci. Rev. 145, 82–93.

Sandweiss, D.H., Maasch, K.A., Burger, R.L., Richardson III, J.B., Rollins, H.B., Clement, A., 2001. Variation in Holocene El Nino frequencies: climate records and cultural consequences in ancient Peru. Geology 29 (7), 603–606.

Saurer, M., Siegwolf, R.T., Schweingruber, F.H., 2004. Carbon isotope discrimination indicates improving water-use efficiency of trees in northern Eurasia over the last 100 years. Glob. Chang. Biol. 10 (12), 2109–2120.

Scheihing, K.W., Moya, C.E., Tröger, U., 2017. Insights into Andean slope hydrology: reservoir characteristics of the thermal Pica spring system, Pampa del Tamarugal, northern Chile. Hydrogeol. J. 25 (6), 1833–1852.

Scheihing, K.W., Moya, C.E., Tröger, U., 2018. Insights into Andean slope hydrology: reservoir characteristics of the thermal Pica spring system, Pampa del Tamarugal, northern Chile. Hydrogeol. J. 1–20.

Schubert, B.A., Jahren, A.H., 2011. Quantifying seasonal precipitation using high–-resolution carbon isotope analyses in evergreen wood. Geochem. Cosmochim. Acta 75 (22), 7291–7303. https://doi.org/10.1016/j.gca.2011.08.002.

Schubert, B.A., Jahren, A.H., 2013. Reconciliation of marine and terrestrial carbon isotope excursions based on changing atmospheric CO2 levels. Nat. Commun. 4https://doi.org/10.1038/ncomms2659. 1653–17.

Schubert, B.A., Jahren, A.H., Eberle, J.J., Sternberg, L.S.L., Eberth, D.A., 2012. A summertime rainy season in the Arctic forests of the Eocene. Geology 40 (6), 523–526. https://doi.org/10.1130/G32856.1.

Shin, S.–I., Sardeshmukh, P.D., Webb, R.S., Oglesby, R.J., Barsugli, J.J., 2006. Understanding the mid–Holocene climate. J. Clim. 19 (12), 2801–2817. https://doi.org/10.1175/jcli3733.1.

Sternberg, L., Deniro, M.J., 1983. Isotopic composition of cellulose from C 3, C 4, and CAM plants growing near one another. Science 220 (4600), 947–949.

Stríkis, N.M., Cruz, F.W., Cheng, H., Karmann, I., Edwards, R.L., Vuille, M., Auler, A.S., 2011. Abrupt variations in South American monsoon rainfall during the Holocene based on a speleothem record from central-eastern Brazil. Geology 39 (11), 1075–1078.

Tapia, P.M., Fritz, S.C., Baker, P.A., Seltzer, G.O., Dunbar, R.B., 2003. A Late Quaternary diatom record of tropical climatic history from Lake Titicaca (Peru and Bolivia). Palaeogeogr. Palaeoclimatol. Palaeoecol. 194 (1), 139–164.

Thompson, L.G., Davis, M.E., Mosley–Thompson, E., Sowers, T.A., Henderson, K.A., Zagorodnov, V.S., et al., 1998. A 25,000–year tropical climate history from Bolivian ice cores. Science 282 (5395), 1858–1864.

Thompson, L.G., Mosley–Thompson, E., Davis, M.E., Lin, P.N., Henderson, K., Mashiotta, T.A., 2003. Tropical glacier and ice core evidence of climate change on annual to millennial time scales. Clim. Change 59 (1/2), 137–155. https://doi.org/10.1023/A:1024472313775.

Thompson, L.G., Mosley-Thompson, E., Davis, M.E., Porter, S.E., 2017. Ice core records of climate and environmental variability in the tropical Andes of Peru: past, present and future. Revista de Glaciares y Ecosistemas de Montaña 3 16–16.

Tomlinson, A., Blanco, N., Ladino, M., 2015. Carta Mamiña, Región de Tarapacá. Servicio Nacional de Geología y Minería. Carta Geológica de Chile, Serie Geología Básica, vol. 1.

Treydte, K., Schleser, G.H., Schweingruber, F.H., Winiger, M., 2016. The climatic significance of $\delta^{13}C$ in subalpine spruces (Lötschental, Swiss Alps). Tellus B 53 (5), 593–611. https://doi.org/10.3402/tellusb.v53i5.16639.

Trobok, V.S., 1984. Fruit and seed morphology of Chilean Prosopis (Fabacae-mimosoideae). In: Habit, M.A. (Ed.), Presented at the International Round Table on Prosopis Tamarugo Phil, pp. 37–39 Arica, Chile.

Urbina Araya, S., Adán Alfaro, L., Pellegrino Hurtado, C., 2012. Arquitecturas formativas de las quebradas de Guatacondo y Tarapacá a través del proceso aldeano (ca. 900 AC-1000 DC). Boletín del Museo Chileno de Arte Precolombino 17 (1), 31–60.

Uribe, M., 2006. In: Lechtman, H. (Ed.), Esferas de Interacción Prehistóricas y Fronteras Nacionales Modernas: Los Andes Sur centrales. Instituto de Estudios Peruanos e Institute of Andean research, pp. 449–502.

Vimeux, F., Ginot, P., Schwikowski, M., Vuille, M., Hoffmann, G., Thompson, L.G., Schotterer, U., 2009. Climate variability during the last 1000 years inferred from Andean ice cores: a review of methodology and recent results. Palaeogeogr. Palaeoclimatol. Palaeoecol. 281 (3–4), 229–241.

Voelker, S.L., Stambaugh, M.C., Guyette, R.P., Feng, X., Grimley, D.A., Leavitt, S.W., Panyushkina, I., Grimm, E.C., Marsicek, J.P., Shuman, B., Curry, B.B., 2015. Deglacial hydroclimate of midcontinental North America. Quat. Res. 83 (2), 336–344.

Vuille, M., 1999. Atmospheric circulation over the Bolivian Altiplano during dry and wet periods and extreme phases of the Southern Oscillation. Int. J. Climatol. A J. R. Meteorol. Soc. 19 (14), 1579–1600.

Vuille, M., Keimig, F., 2004. Interannual variability of summertime convective cloudiness and precipitation in the central Andes derived from ISCCP–B3 data. J. Clim. 17 (17), 3334–3348.

Vuille, M., Werner, M., 2005. Stable isotopes in precipitation recording South American summer monsoon and ENSO variability: observations and model results. Clim. Dyn. 25 (4), 401–413.

Vuille, M., Bradley, R.S., Keimig, F., 2000. Interannual climate variability in the Central Andes and its relation to tropical Pacific and Atlantic forcing. J. Geophys. Res. Atmosphere 105 (D10), 12447–12460.

Vuille, M., Bradley, R.S., Werner, M., Healy, R., Keimig, F., 2003a. Modeling δ18O in precipitation over the tropical Americas: 1. Interannual variability and climatic controls. J. Geophys. Res. Atmosphere 108 (D6).

Vuille, M., Bradley, R.S., Healy, R., Werner, M., Hardy, D.R., Thompson, L.G., Keimig, F., 2003b. Modeling δ18O in precipitation over the tropical Americas: 2. Simulation of the stable isotope signal in Andean ice cores. J. Geophys. Res.: Atmosphere 108 D6.

Vuille, M., Burns, S.J., Taylor, B.L., Cruz, F.W., Bird, B.W., Abbott, M.B., Novello, V.F., 2012. A review of the South American monsoon history as recorded in stable isotopic proxies over the past two millennia. Clim. Past 8 (4), 1309–1321.

Winterholder, B., 1980. Environmental analysis in human evolution and adaptation research. Hum. Ecol. 8, 135–170.

Winterholder, B., Thomas, B., 1978. Geoecology of Southern Highland Peru: A Human Adaptation Perspective. Institute of Arctic and Alpine Research. Occasional Paper No. 27. University of Colorado, Boulder.

Wolfe, B.B., Aravena, R., Abbott, M.B., Seltzer, G.O., 2001. Reconstruction of paleohydrology and paleohumidity from oxygen isotope records in the Bolivian Andes. Palaeogeography 176 (1–4), 177–192. https://doi.org/10.1016/s0031–0182(01)00337–6.

Woodley, E.J., Loader, N.J., McCarroll, D., Young, G.H.F., Robertson, I., Heaton, T.H.E., et al., 2011. High temperature pyrolysis/gas chromatography/isotope ratio mass spectrometry: simultaneous measurement of the stable isotopes of oxygen and carbon in cellulose. Rapid Commun. Mass Spectrom. 26 (2), 109–114. https://doi.org/10.1002/rcm.5302.

Yakir, D., Berry, J.A., Giles, L., Osmond, C.B., 1994. Isotopic heterogeneity of water in transpiring leaves:identification of the component that controls the $\delta^{18}O$ of atmospheric O_2 and CO_2. Plant, Cell Environ. 17 (1), 73–80. https://doi.org/10.1111/j.1365–3040.1994.tb00267.x.

Zhou, J., Lau, K.M., 1998. Does a monsoon climate exist over South America? J. Clim. 11 (5), 1020–1040.